Gastroenterology 2020;159:1853–1865

FXR Isoforms Control Different Metabolic Functions in Liver Cells via Binding to Specific DNA Motifs

Jose Miguel Ramos Pittol,[1,2] Alexandra Milona,[3] Imogen Morris,[1] Ellen C. L. Willemsen,[1] Suzanne W. van der Veen,[1] Eric Kalkhoven,[1] and Saskia W. C. van Mil[1]

[1]Center for Molecular Medicine, University Medical Center Utrecht, Utrecht University, Utrecht, the Netherlands; [2]Institute of Biochemistry and Center for Molecular Biosciences Innsbruck, University of Innsbruck, Innsbruck, Austria; and [3]Medical Research Council, London Institute of Medical Sciences, Institute of Clinical Sciences, Faculty of Medicine, Imperial College London, London, United Kingdom

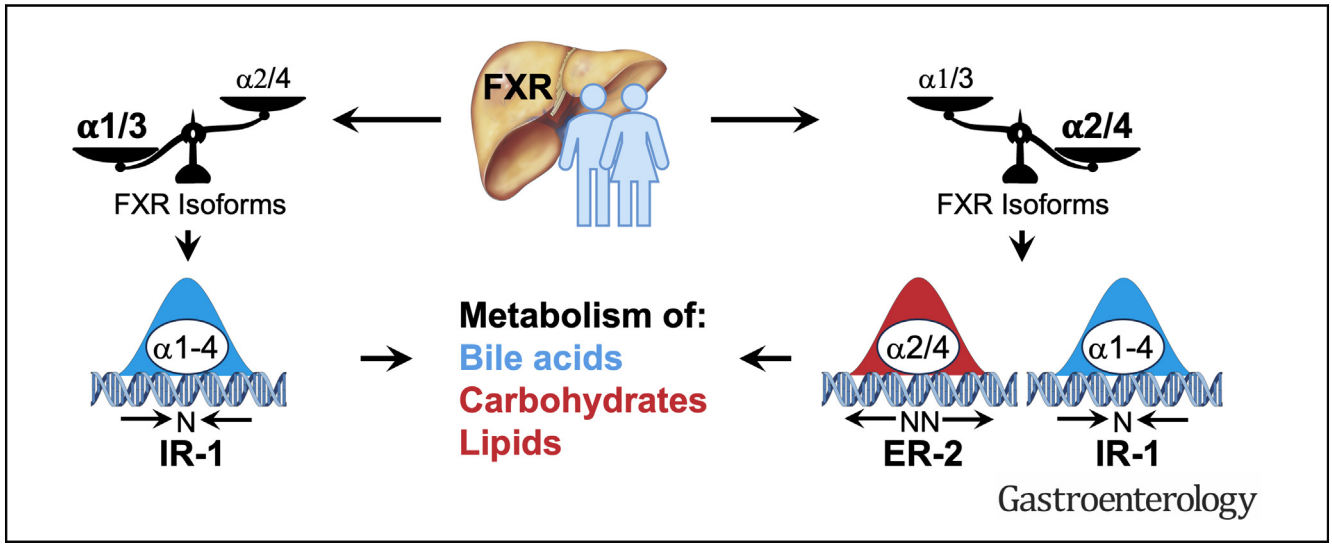

See editorial on page 1655.

BACKGROUND & AIMS: The nuclear receptor subfamily 1 group H member 4 (NR1H4, also called FXR) is a ligand-activated transcription factor that, upon binding of bile acids, regulates the expression of genes involved in bile acid, fat, sugar, and amino acid metabolism. Transcript variants encode the FXR isoforms alpha 1, alpha 2, alpha 3, and alpha 4, which activate different genes that regulate metabolism. Little is known about the mechanisms by which the different isoforms regulate specific genes or how the expression of these genes affects the outcomes of patients given drugs that target FXR. **METHODS:** We determined genome-wide binding of FXR isoforms in mouse liver organoids that express individual FXR isoforms using chromatin immunoprecipitation, followed by sequencing analysis and DNA motif discovery. We validated regulatory DNA sequences by mobility shift assays and with luciferase reporters using mouse and human FXR isoforms. We analyzed mouse liver organoids and HepG2 cells that expressed the FXR isoforms using chromatin immunoprecipitation, quantitative polymerase chain reaction, and immunoblot assays. Organoids were analyzed for mitochondrial respiration, lipid droplet content, and triglyceride excretion. We used the FXR ligand obeticholic acid to induce FXR activity in organoids, cell lines, and mice. We collected data on the binding of FXR in mouse liver and the expression levels of FXR isoforms and gene targets in human liver tissue and primary human hepatocytes from the Gene Expression Omnibus. **RESULTS:** In mouse liver cells, 89% of sites that bound FXR were bound by only FXRα2 or FXRα4, via direct interactions with the DNA sequence motif ER-2. Via DNA binding, these isoforms regulated metabolic functions in liver cells, including carbon metabolism and lipogenesis. Incubation with obeticholic acid increased mitochondrial pyruvate transport and reduced insulin-induced lipogenesis in organoids that expressed FXRα2 but not FXRα1. In human liver tissues, levels of FXRα2 varied significantly and correlated with expression of genes predicted to be regulated via an ER-2 motif. **CONCLUSIONS:** Most metabolic effects regulated by FXR in mouse and human liver cells are regulated by the FXRα2 isoform via specific binding to ER-2 motifs. The expression level of FXRα2 in liver might be used to predict responses of patients to treatment with FXR agonists.

Keywords: OCA; Fatty Liver; Steatosis; NASH.

Abbreviations used in this paper: **AU, Arbitrary units; ChIP, chromatin immunoprecipitation; ChIP-seq, chromatin immunoprecipitation sequencing; DMEM, Dulbecco's modified Eagle medium; DMSO, dimethyl sulfoxide; ER-2, everted hexamer repeat spaced by 2 nucleotides; FXR, farnesoid X receptor; GFP, green fluorescent protein; HCC, hepatocellular carcinoma; Ibabp, ileal bile acid binding pump; IR-1, inverted hexamer repeat spaced by 1 nucleotide; kb, kilo base pairs; MPC, mitochondrial pyruvate carrier; Mpc1, mitochondrial pyruvate carrier 1; NASH, nonalcoholic steatohepatitis; OCA, obeticholic acid; PBS, phosphate-buffered saline; PCR, polymerase chain reaction; q, quartile; qPCR, quantitative polymerase chain reaction; PHH, primary human hepatocytes; RLU, Relative luciferase units; RNA-seq, RNA sequencing; Shp, small heterodimeric partner; TG, triglycerides; wt, wild type.**

Most current article

0016-5085
https://doi.org/10.1053/j.gastro.2020.07.036

The nuclear receptor subfamily 1 group H member 4 (NR1H4, also called FXR) is a transcription factor belonging to the superfamily of nuclear receptors.[1–3] Upon binding bile acids, FXR activates transcription of genes involved in the repression of de novo lipogenesis and gluconeogenesis, ammonia detoxification, promotion of glycogen synthesis, and bile acid metabolism.[4,5] In addition, we and others have shown that FXR activation reduces inflammation.[6] *Fxr*$^{-/-}$ mice develop nonalcoholic fatty liver disease, nonalcoholic steatohepatitis (NASH), fibrosis, and spontaneous hepatocellular carcinoma (HCC),[7,8] highlighting the relevance of FXR in the homeostasis of the healthy liver. On this basis, FXR agonists are currently used for the treatment of primary biliary cholangitis and are being tested in clinical trials for multiple metabolic and gastrointestinal diseases, including type 2 diabetes, metabolic syndrome, and NASH.[9] FXR is expressed as 4 different isoforms from a single locus in both humans and mice. The isoforms, alpha1 to alpha4, differ in their activation function domain 1 (AF-1) at the N-terminus and in the presence of a 4–amino acid extension (MYTG) of the DNA binding domain (DBD) (Figure 1*A*). The 2 promoters driving FXR expression are differentially active among tissues; however, every FXR-expressing cell contains a proportion of MYTG-positive (α1 or α3) and -negative (α2 or α4) FXR derived from an alternative splicing event. Human livers, for example, predominantly express *FXRα1* and *α2.*[10] Intriguingly, the *FXRα2/FXRα1* expression ratio in the liver is lower in both histologically normal and tumor tissue of patients with HCC compared to healthy liver tissue.[11] Correia et al[12] have shown that fasting and exercise acutely increase the *Fxrα2/Fxrα1* expression ratio. Based on adenoviral overexpression of single FXR isoforms in *Fxr*$^{-/-}$ mice, they also propose that FXRα2 may be beneficial in the promotion of hepatic lipid clearance through an isoform-specific gene expression profile. However, it is not yet possible to translate this information for patient stratification or the development of therapeutics because the mechanisms behind FXR isoform-specific activation remain undiscovered. Here, we show that FXRα2 and α4 are the dominating isoforms in the response to FXR agonism on the basis of DNA binding frequency and the number of downstream target genes. Genome-wide, 89% of sites that bound FXR were bound by only FXRα2 or FXRα4. To our surprise, this isoform selectivity is achieved through binding to an ER-2 (everted hexamer repeat spaced by 2 nucleotides) DNA motif, in addition to the canonical FXR binding motif (IR-1 [inverted hexamer repeat spaced by 1 nucleotide]). As a result, FXRα2 or α4 are responsible for the majority of the transcriptional effects derived from agonist treatment and their subsequent metabolic effects. In human liver biopsy specimens, levels of FXRα2 varied significantly and correlated with the expression of genes predicted to be regulated via an ER-2 motif. We conclude that FXRα2 expression dominates the effects of FXR agonism via ER-2 binding and that its expression influences liver metabolism and treatment efficacy for metabolic diseases.

WHAT YOU NEED TO KNOW

BACKGROUND AND CONTEXT

FXR binds to bile acids to regulate expression of genes involved in bile acid, glucose, fat, and amino acid metabolism. Transcript variants encode the isoforms alpha1, alpha2, alpha3, and alpha4.

NEW FINDINGS

Most metabolic effects regulated by FXR in mouse and human liver cells depend on expression of the FXRα2 or FXRα4 isoform. These isoforms bind to a genome-wide DNA motif, named ER-2.

LIMITATIONS

Further studies are needed of differences in expression in FXR isoforms and their effects on function in animal models of disease and in humans.

IMPACT

Hepatic expression levels of FXRα2 might be used to predict patient responses to FXR agonists.

Methods

Materials

Polyclonal antibody against FXR (Santa Cruz Biotechnology, Dallas, TX; sc-13063) was used for chromatin immunoprecipitation (ChIP) experiments. Monoclonal antibodies against β-actin (Abcam, Cambridge, UK; ab8224) and FXR (Invitrogen, Carlsbad, CA; 417200) were used for Western blot. Obeticholic acid (OCA) was kindly provided by Intercept Pharmaceuticals, Inc (New York, NY).

Plasmids

Coding sequences from human FXR isoforms α1 (NM_001206977.2), α2 (NM_005123.4), α3 (NM_001206993.2), and α4 (NM_001206992.2) were amplified from human complementary DNA. Mouse homologue coding sequences were a gift from Prof. Bert Groen. All FXR variants were amplified by polymerase chain reaction (PCR) and cloned into vectors containing a myc-TwinStrep or HA-tag at their C-terminus. FXR isoforms from mouse were transduced in organoids by using pLV(PGK1)-IRES-Puro, or pLV(PGK1)-IRES-Neo in the short hairpin RNA experiments. Mouse Nr0b2 (also known as Shp) was knocked down by short hairpin RNA (shRNA) using pLKO.1 clone TRCN0000027046 (Sigma MISSION shRNA). SHC002 (Sigma-Aldrich, St Louis, MO) was used as control (ctrl). Reporter plasmids containing different motifs/regions were based on pGL3[MinP/Luc2] (Promega, Madison, WI) (Supplementary Figure 1*B*). The mouse Shp enhancer (Shp_e) and Fabp4 (also known as ileal bile acid binding pump [Ibabp]) promoter were amplified from mouse genomic DNA by PCR and subcloned on the pGL3[MinP/Luc2]. Mouse-derived coordinates and sequence features are provided in Supplementary Table 1.

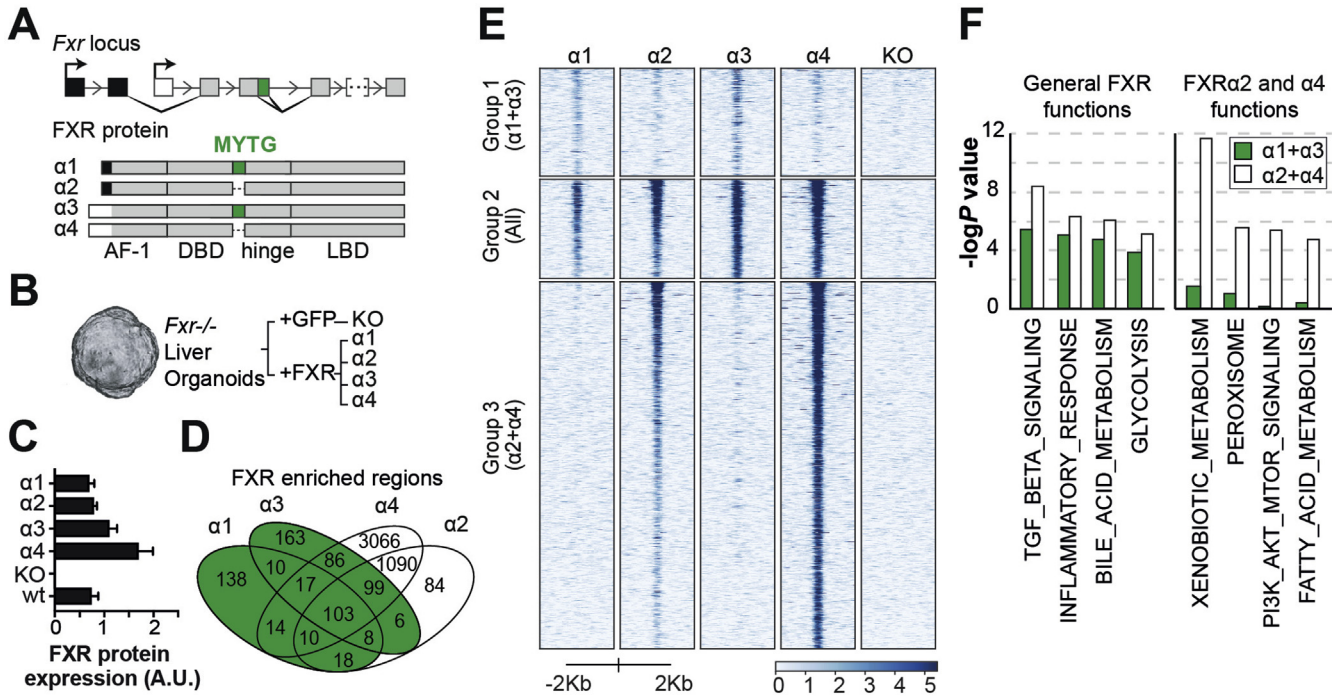

Figure 1. FXRα2 and α4 control the majority of FXR functions through isoform-specific DNA binding. (*A*) Gene and protein organization of FXR isoforms in humans and mice. (*B*) Schematic representation of the generation of liver organoid lines expressing single FXR isoforms. (*C*) Quantification of FXR expression in organoid lines by Western blot, FXR/glyceraldehyde-3-phosphate dehydrogenase (GAPDH) (see Supplementary Figure 2*B*) Bars represent standard deviation. (*D*) Venn diagram of ChIP-seq peak overlaps between FXR isoforms. Statistics are listed in Supplementary Table 2. (*E*) Heatmap of FXR occupancy in ChIP-seq peaks grouped by isoform overlap. For group 3, 1000 random peaks are displayed. (*F*) Hallmark pathway analysis of genes with neighboring FXR bound regions.

Mice

Studies were approved by the University Medical Center Utrecht ethics committee and conducted in accordance with European law. The 9–12-week-old male C57BL/6 wild-type (wt) and *Fxr*$^{-/-}$ mice[13] were housed in a room with controlled temperature (20–24°C), relative humidity (55% ± 15%), and a 12-h light/dark cycle. Mice were fed chow and water ad libitum. Mice received either a treatment with OCA (10 mg/kg/day) or vehicle (1% methyl cellulose) daily by oral gavage for 7 days. On the last day, the food was removed in the morning, and the mice received a final dose of OCA or vehicle. Livers/plasma were harvested after 4 hours.

Cell and Organoid Culture

HEK-293T were grown in Dulbecco's modified Eagle medium (DMEM) (Lonza, Basel, Switzerland; 12-604F) supplemented with 10% fetal bovine serum (Bodinco BV, Alkmaar, Netherlands). HepG2 cells were grown in DMEM (Lonza, 12-707F) supplemented with L-glutamine (Lonza, 17-605E), Penicillin/Streptomycin, and 10% fetal bovine serum. Liver organoids from *wt* and *Fxr*$^{-/-}$ mice were generated, expanded, and differentiated as previously described.[14] Transduced HepG2 and organoid lines were generated with third-generation lentiviral vectors by using supernatants from HEK-293T cells cotransfected with lentiviral packaging mix (Sigma-Aldrich).

Luciferase Reporter Assays

HEK-293T cells were transfected using polyethylenimine in a 96-well plate format; 2 ng pCDNA3.1-RXRA-Flag, 5 ng pGL3 reporter, and 2 ng TK-*Renilla* were used consistently throughout the experiments. Unless otherwise stated, 10 ng of pCDNA3.1-expressing tagged human FXR isoforms or green fluorescent protein (GFP) were used. At 24 hours after transfection, cells were incubated with dimethyl sulfoxide (DMSO) and 5 μmol/L OCA overnight. Cells were thereafter lysed, and firefly and *Renilla* luciferase activity were measured with the Dual-Luciferase Reporter Assay System (Promega, E1960) in a TriStar2 LB942 Multimode Reader (Berthold Technologies, Bad Wildbad, Germany). Results are expressed as Relative Luciferase Units (RLU), according to the providers protocol. Each n represents an independent treatment of 3 separate transfected wells.

Electrophoretic Mobility Shift Assays

Tagged FXR isoforms from mouse and human, RXRα, and GFP proteins were in vitro translated from pCDNA3.1 vectors by using the TNT Quick Coupled Transcription/Translation system (Promega). Binding reactions and detection were performed as described previously.[15]

Bioenergetic Measurements

The Seahorse Bioscience (Billerica, MA) XFe24 Analyzer was used to measure oxygen consumption rates in picomoles of O_2 per minute. Differentiated liver organoids were seeded in 3 μL Matrigel (Corning, New York, NY) per well in XF24 cell culture microplates and treated overnight with DMSO or 5 μmol/L OCA in fresh differentiation medium. One hour before the measurements, culture medium was replaced with

Seahorse XF Base medium, supplemented with 20 mmol/L glucose, 2 mmol/L L-glutamine, 5 mmol/L pyruvate, and 0.56 μL 1 mol/L NaOH, and the plate was incubated for 60 minutes at 37 °C. Depending on the experiment, either pyruvate was omitted or 10 μmol/L of mitochondrial pyruvate carrier (MPC) inhibitor UK5099 was added. During the assay, 5 μmol/L oligomycin, 2 μmol/L trifluoromethoxy carbonylcyanide phenylhydrazone (FCCP), and 1 μmol/L of rotenone and antimycin A were injected to each well after 18, 45, and 63 minutes, respectively. After injections, measurements of 2 minutes were performed in triplicate, preceded by 4 minutes of mixture time. All chemicals were purchased from Sigma-Aldrich.

Lipid Accumulation Assays

Differentiated liver organoids were treated overnight with DMSO or 5 μmol/L OCA in fresh differentiation medium. Afterward, the organoids were washed 2 times with phosphate-buffered saline (PBS), and the medium was replaced with fasting medium (DMEM-F12 no phenol red [Gibco, Waltham, MA; 21041-025], B27 supplement minus insulin [Gibco, A1895601], 30 μmol/L dexamethasone [Sigma-Aldrich, D4902], and 10 μmol/L forskolin [Sigma-Aldrich, F6886]). After 4 hours, the organoids were washed 2 times with PBS and treated with fresh insulin medium (DMEM-F12 no phenol red, B27 supplement [Gibco, 17504044] and 30 μmol/L dexamethasone). Medium samples were taken for triglyceride (TG) excretion measurement after 2, 6 and 8 hours. Peak secreted values are reported in graphs, typically at 2 hours. Genomic DNA was used for the normalization for cell numbers. For visualization of intracellular lipid accumulation, the organoids were treated as described, fixed in 4% paraformaldehyde after 8 hours, sealed, and stored at 4°C.

Triglyceride Measurement

TG from mice plasma was quantified with the Triglyceride GPO reagent in conjunction with the SYNCHRON LX system (Beckman Coulter, Brea, CA). For the determination of TG in culture media, Triglycerides Liquicolor Mono Kit (HUMAN, Wiesbaden, Germany) was used. Absorbance at 500 and 650 nm was measured on a SpectraMax m5 (Molecular Devices, San Jose, CA). A titration of the standard provided with the kit was used to accurately assess low TG amounts.

Imaging of Lipid Staining in Liver Organoids

Fixed organoids were washed in PBS and permeabilized by using 0.5% Tween20 for 15 minutes. Organoids were stained with Hoechst 3334 2 μg/m: and LipidTOX Green Neutral Lipid Stain (1:500, Invitrogen) for 20 minutes at room temperature. All samples were mounted in Fluoromount and imaged on a Zeiss (Oberkochen, Germany) laser scanning microscope (LSM) 510 META within 1 hour of staining at room temperature. Images were acquired using a Zeiss LSM 510 META confocal microscope (LSM software ZEN 2009, Zeiss) using a Plan-Neofluar 40×/1.30 oil objective lens. All images were processed by using ImageJ (National Institutes of Health, Bethesda, MD).[16] Images shown are representative of 3 independent experiments.

Chromatin Immunoprecipitation Followed by Sequencing or Quantitative Polymerase Chain Reaction

FXR occupancy was assessed in differentiated, single isoform–expressing organoids after 1 hour of incubation with 5 μmol/L OCA. ChIP for FXR was performed according to Ramos-Pittol et al.[17] Purified DNA was either used for quantitative PCR (qPCR) or for next-generation sequencing.

Sequencing libraries were generated by using the NEXTflex Rapid DNA-seq Kit (Bio Scientific, Phoenix, AZ) by using approximately 0.5 ng ChIP or genomic DNA. Sequencing was performed in the Nextseq500 platform (Illumina; single-end, 75–base pair reads). ChIP sequencing (ChIP-seq) reads were aligned to the mouse reference genome mm9 by using bowtie2.[18] Enriched regions were identified by using MACS 1.4.[19] Coverage was computed with DeepTools2,[20] bamCoverage with options "–binsize 50 –normalizeUsing RPGC –effectiveGenomeSize 1865500000 –extendReads 300." Input tracks were thereafter subtracted by using bigwigCompare. For the heatmap display, computeMatrix was used on regions defined by MACS overlap, with options "–referencePoint center -a 2000 -b 2000 -bs 50." Known and de novo enriched DNA motifs at ChIP-seq peaks were identified by using HOMER[21] findmotifsgenome with -len either "7,14" or "20." Venn diagrams and the significance of region overlaps were calculated with Bioconductor ChIPpeakAnno[22] makeVenndiagram, with option "totaltest=6000."

HOMER annotatepeaks was used to define promoters with an FXR peak within 10 kilo base pairs (kb), and to perform Gene Ontology term analysis. A threshold value of 8 was used for the detection of motifs in candidate regions. Hallmark pathways were selected from the msigdb set.[23] Motif score threshold was reduced by 1 for both ER-2 and IR-1 for detection within FXR peak regions. Randomized regions were obtained with the bash command gsort with option "-R".

RNA Isolation

Liver organoids were differentiated into the hepatocyte lineage[14] and treated with either DMSO or 5 μmol/L OCA for 8 hours before RNA extraction. RNA was isolated by using TRIzol reagent (Ambion/Life Technologies, Naugatuck, CT) and further processed for reverse transcription (RT) using iScript (Bio-Rad, Hercules, CA; 1708891) or for next-generation sequencing; n represents an independently differentiated organoid experiment.

RNA Sequencing

Libraries were generated by using NEXTflex Rapid RNA-seq Kit using 1 μg total RNA. Sequencing was performed in the Nextseq500 platform (Illumina; single-end, 75–base pair reads). RNA-sequencing (RNA-seq) reads were aligned to the reference genomes mm9 or hg19, for organoids and HepG2 respectively, by using Tophat 2.18.[24] Differential expression of genes was assessed by using Cufflinks.[25]

Quantitative Polymerase Chain Reaction

qPCR was performed on a CFX384 Real-Time system by using FastStart Universal SYBR Green Master Mix (ROX) (Roche, Indianapolis, IN; 4913850001). Primer pairs were designed with the Roche ProbeFinder qPCR design tool. In the experiments where qPCR was performed following reverse transcription (RT-qPCR), the gene peptidyl-prolyl cis-trans isomerase (Ppia) was used for sample normalization. Primer sequences can be found in Supplementary Table 4; n represents an independent RNA or DNA sample.

Gene Expression Omnibus Data Sets

ChIP-seq data for FXR in mouse livers (GSE73624)[26] and RNA-seq data from human liver tissue (GSE77509)[27] and from primary human hepatocytes (PHHs) (GSE57227)[28] were accessed through the Gene Expression Omnibus.[29] Specific samples analyzed can be found in Supplementary Table 5. For the comparison of FXR expression among different sources (patients, HepG2, and PHH), reads aligned to chromosome 5 were used for quantification and normalization of transcripts with HTseq 0.11.1[30] and Deseq2(3.9).[31] The normalized reads provided in the Gene Expression Omnibus accession were used for the sorting of patients by FXR expression and reporting of respective FXR targets. Bedtools intersect[32] was used for the quantification of reads surrounding the MYTG alternative splicing site.

Data Availability

The gene expression and FXR occupancy data that support the findings of this study are deposited at the NCBI Gene Expression Omnibus database under accession codes GSE133659, GSE133700, and GSE133734.

Statistics Software

GraphPad Prism software, version 8.1.2 (227) (GraphPad Software, Inc, San Diego, CA) was used for figure preparation and statistical analysis. Applied tests and independent replicates per subgroup (n) are reported in figure legends. Analysis of variance (ANOVA) and *t* tests considered 2-tailed *P*-values. *P* values of $<.05$ were considered statistically significant. Unless otherwise stated, error bars represent Standard Error of the Mean (SEM).

Results

FXRα2 and α4 Control the Majority of FXR Functions Through Isoform-Specific DNA Binding

As a model to study FXR isoform-selective effects, single FXR isoforms were transduced into liver organoids derived from *Fxr*$^{-/-}$ mice (Figure 1*B*). Expression of the reintroduced isoforms was comparable with the FXR expression in organoids derived from wt mice (Figure 1*C* and Supplementary Figure 2*A* and *B*). To investigate whether differential DNA binding plays a role in FXR isoform specificity, we performed ChIP for FXR on the reconstituted liver organoid lines, followed by next-generation sequencing. From this assay, we determined that 89% of all FXR peaks were selectively bound by FXRα2 and α4 (Figure 1*D* and *E* and Supplementary Figure 2*C*). DNA binding by FXRα4 appears more robust overall, in agreement with higher expression of this isoform in the respective organoid line. For further analysis, peaks were grouped based on binding by FXRα1 and α3 (group 1), by all 4 isoforms (group 2), or by FXRα2 and α4 (group 3) (Figure 1*E*). To assess the potential functional role of these binding events, we performed hallmark pathway analysis on genes located within 10 kb from an FXR binding peak (Figure 1*F*). Focusing on FXR-related terms, we discovered a strong difference between isoforms. Although genes related to bile acid metabolism and inflammatory response were regulated by all isoforms, xenobiotic and fatty acid metabolism were highly specific to FXRα2 and α4. Moreover, all significantly enriched pathways within FXRα1 and α3 targets were shared among all the isoforms (see Supplemental Material). These results forecast the dominance of isoforms α2 and α4 with regard to the FXR response and show a segregation of functions through isoform-specific DNA binding.

ER-2 Motifs Are Exclusively Bound by FXRα2 and α4

To assess whether specific DNA sequences were responsible for the differences in isoform binding, we generated de novo DNA motifs based on the FXR peaks that were differentially bound by the isoforms (Figure 1*D*). For groups 1 and 2, the canonical IR-1 motif was the most enriched. Group 3, however, was highest enriched for an ER-2 motif (Figure 2*A*). Although seemingly similar, we found

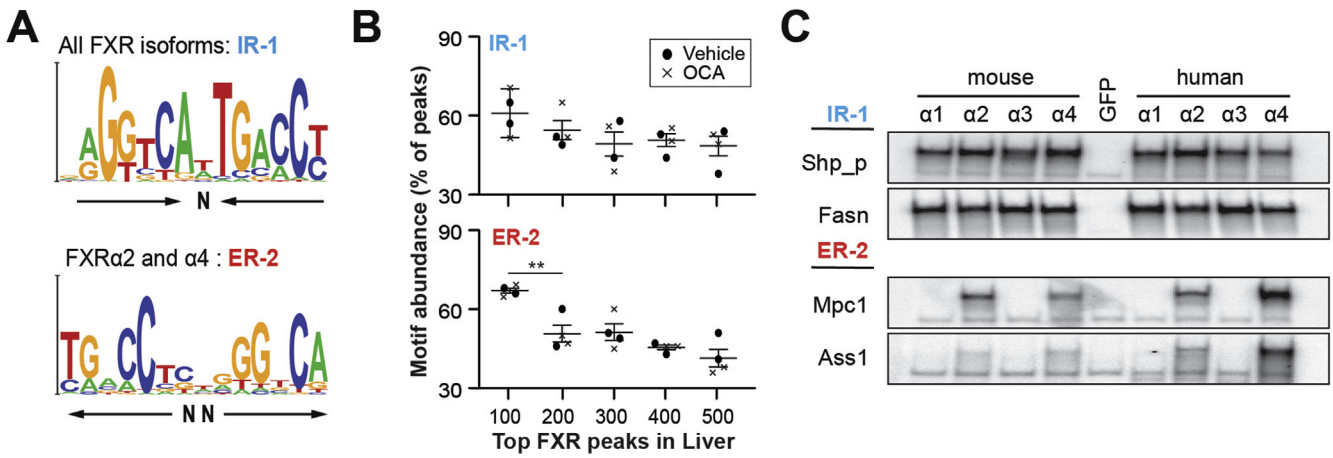

Figure 2. ER-2 motifs are exclusively bound by FXRα2 and α4. (*A*) The top represented de novo motifs in FXR peak groups 1/2 (all FXR isoforms) and 3 (FXRα2 and α4). Arrows represent the orientation of hexameric repeats. (*B*) Comparative abundances of the IR-1 and ER-2 motifs in FXR peaks from mouse livers (GSE73624). Circles indicate vehicle-treated mice; crosses represent OCA-treated mice. (*C*) Interaction of human and mouse FXR isoforms with naturally occurring IR-1 and ER-2 motif probes by electromobility shift assays. Graphs (*B*) show the average and SEM from 4 FXR ChIP-seq data sets. Data were compared by using ANOVA/Sidak vs the following ranked peak group. $^{**}P \leq .01$.

no correlation between the scores for both motifs within the FXR peaks. Group 1 and 2 peaks scored high for IR-1, whereas group 3 scored high for ER-2 (Supplementary Figure 3*A*). Regarding their location within the peaks, both IR-1 and ER-2 motifs were found in the proximity of the peak summits, suggesting direct binding (Supplementary Figure 3*B*).

To validate our findings in mouse liver, we analyzed liver FXR binding peaks from mice treated with vehicle or OCA (GSE73624). For each mouse sample, peaks were sorted according to significance of FXR enrichment, separated in bins of 100 peaks, and analyzed for the presence of either motif. We detected significant abundance of the ER-2 in FXR bound regions, comparable to that of the canonical FXR binding motif IR-1 (Figure 2*B*, Supplementary Figure 3*C*, Supplementary Table 6). Interestingly, the presence of the ER-2 was especially marked within the top 100 FXR peaks in every data set analyzed, independent of ligand treatment. We conclude that FXR also binds to the ER-2 in vivo, which may contribute to the frequency of binding events to regulatory regions.

To test whether FXRα2 and α4 isoforms are responsible for the binding observed in ER-2–containing regions, we analyzed FXR isoform binding to selected IR-1 and ER-2 native motifs in electrophoretic mobility shift assays (EMSA). As reported previously,[33] all isoforms, both human and mouse, bind to IR-1 motif probes. In contrast, only FXRα2 and α4 bind to the ER-2 motifs (Figure 2*C* and Supplementary Figure 3*D*). We conclude that the binding of FXRα2 and α4 to the ER-2 motif is direct, which is likely to contribute to increased FXR occupancy in specific genomic regions.

ER-2–Containing Regions Are Selectively Regulated by FXRα2 and α4

Next, we tested the effects of the IR-1 or ER-2 sequences within regulatory regions on the activation of transcription by FXR isoforms transcriptome-wide. We classified all potential FXR target genes according to the presence of each motif at the binding site (FXR peak <10 kb from promoter region) and assessed their fold changes by RNA-seq in liver organoids incubated with OCA (Figure 3*A*). Genes proximal to an IR-1 FXR peak were similarly regulated by FXRα1 and α2. In contrast, the presence of the ER-2 leads to a higher induction by FXRα2. Overall, FXRα3 and FXRα4 showed a comparable pattern (Supplementary Figure 1*A*). Using this approach, we categorized FXR target genes as general, including *Slc51b* (Also known as *Ostβ*) and *Osgin1*, or isoform specific, including *Slc51a* (Also known as *Ostα*), *Ass1*, *Mpc1*, and *Glyctk*.

To investigate whether isoform-specific activation can be achieved through binding to ER-2 motifs, we generated luciferase reporter constructs containing native IR-1 and ER-2 motifs (Figure 3*B*, and Supplementary Figure 1*B*, Supplementary Table 1). We observed that the reporters containing IR-1 motifs, like the one found in the mouse *Shp* promoter (Shp_p), were activated by both FXRα1 and α2. On the other hand, ER-2 containing reporters were only

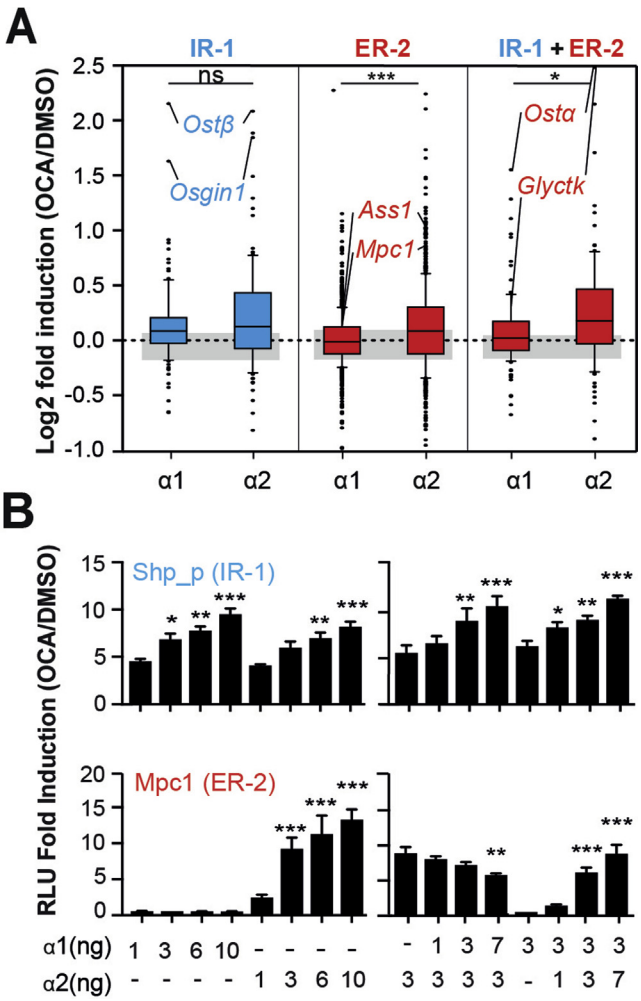

Figure 3. FXRα2, and not FXRα1, activates transcription from ER-2 motifs upon ligand treatment. (*A*) RNA fold induction of genes with neighboring FXR bound regions containing an IR-1, ER-2, or both motifs after incubation with OCA. n = 105 (IR-1), n = 734 (ER-2), and n = 104 (IR-1 + ER-2). Bars represent 10th–90th percentiles. As a reference, the interquartile range for gene induction in knockout organoids is depicted in gray. (*B*) Transcriptional activity of human FXRα1 and α2 on Shp_p (IR-1) and Mpc1 (ER-2) motif reporter constructs after incubation with OCA. FXR isoforms were expressed individually (*left*) or coexpressed at different ratios (*right*). Graphs show group average and SEM, n = 3. Data were compared using the (*A*) Kruskal-Wallis *H* test and (*B*) 2-way ANOVA/Sidak vs 1-ng condition (*left*) or vs single isoform group control (*right*). *$P \leq .05$, **$P \leq .01$, ***$P \leq .001$. ns = not significant.

activated by FXRα2. A comparable isoform specificity was observed for additional motif reporters (Supplementary Figure 1*C*). Considering that FXRα1 and α2 are coexpressed in the liver, we tested the effect of changes in FXR amounts, and their isoform ratio, on the transcriptional activation from IR-1 and ER-2 sequences (Figure 3*B*, *right*). For the IR-1 reporter, the total amount of FXR transfected dictated the fold induction upon incubation with OCA, regardless of the isoform ratio. For the ER-2 reporter, the activation depended on the amount of FXRα2 alone. However, high FXRα1 expression seems to reduce FXRα2

transactivation. Currently, we have no explanation for this. We speculate that competition for coactivators may play a role. In summary, we conclude that FXRα2 binding to ER-2 motifs genome wide results in isoform-specific transcriptional effects. Additionally, the magnitude of the activation from ER-2 motifs upon incubation with OCA depends on FXRα2 expression.

FXRα2 Activation Increases Mitochondrial Respiratory Capacity Through Mpc1

Among the novel FXR isoform-specific target genes, we found the mitochondrial pyruvate carrier 1 (Mpc1) (Figure 4*A*). Mpc1 mediates pyruvate transport to the mitochondrial matrix, increasing the influx of carbon to the tricarboxilic acid (TCA) cycle and affecting mitochondrial function (Figure 4*B*). To assess whether FXR-driven Mpc1 increases influx into the trichloroacetic acid cycle, we performed a Mito Stress Assay (Seahorse) in which the oxygen consumption rate after specific drug treatments reflects general mitochondrial function. For simplicity, we limited further experiments to FXRα1 and α2, because these are the predominant isoforms in human liver. The incubation of wt liver organoids with OCA resulted in an increase of the spare respiratory capacity, not seen in *Fxr*$^{-/-}$ organoids (Figure 4*C*). Only FXRα2-expressing organoids showed this same phenotype. In addition, both removal of pyruvate from the assay medium (Figure 4*D*) or treatment with the Mpc1 inhibitor UK5099 (Figure 4*E*) abolished the effect of OCA. These results confirm the action of Mpc1 downstream of FXRα2 activation, leading to changes in mitochondrial function reflected as an increase in the spare respiratory capacity.

FXRα2-Specific Up-regulation of Shp *Reduces Lipogenesis in Liver Organoids*

Contradictory to our reporter data containing the Shp promoter IR-1 (Figure 2*B*), the expression of Shp in liver organoids is induced stronger by FXRα2 and α4. This is in contrast to *Ostβ*, which is an IR-1–regulated gene (Figure 5*A*). ChIP-seq analysis in the mouse liver organoids showed that the promoter region (Shp_p) is equally bound by all 4 FXR isoforms, but FXRα2 and α4 show stronger binding to an enhancer region at the transcription termination site (Shp_e) (Figure 5*B* and Supplementary Figure 2*D*). Therefore, binding to the Shp_e region is most likely responsible for the isoform specificity in the induction of *Shp* expression. Within this region, we found 2 conserved sites (termed sites 1 and 2) with overlapping IR-1:ER-2 motifs (Figure 5*C* and Supplementary Figure 4*A*). In luciferase reporter constructs containing the Shp_e region, we observed that both sites 1 and 2 contribute to the transcriptional capacity of FXR in an additive manner. Sites 1 and 2 can be activated by both FXR α1 and α2, as predicted by the presence of IR-1, but the up-regulation driven by FXRα2 is stronger in both cases (Figure 5*D*).

Considering the isoform selectivity of the overlapping sites, we hypothesized that these sequences can act as both IR-1 and ER-2 motifs simultaneously. To test this hypothesis, we generated a reporter construct containing the IR1:ER2 composite motif at Site1 of the Shp_e and mutated each of the 3 hexameric repeats (Supplementary Figure 4*B*). Mutation of the IR-1 sequence resulted in exclusive activation by FXRα2, whereas mutation of the ER-2 effectively abrogated isoform selectivity (Supplementary

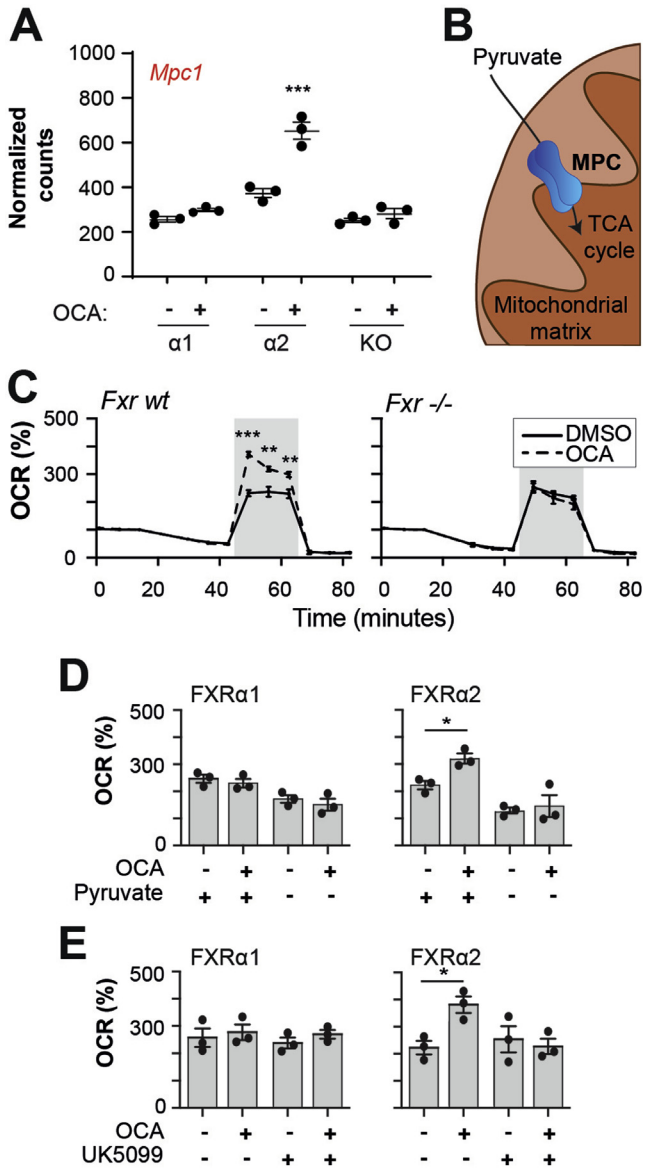

Figure 4. FXRα2 activation increases mitochondrial respiratory capacity through Mpc1. (*A*) Expression of *Mpc1* in liver organoids upon incubation with OCA treatment by RNA-seq. (*B*) Schematic representation of MPC function. (*C*) Mito Stress Kinetic graphs showing baseline oxygen consumption rate in wt and *FXR*$^{-/-}$ organoids incubated with OCA. Spare respiratory capacity measurements are highlighted in gray. (*D*, *E*) Spare respiratory capacity on FXRα1- or FXRα2-expressing organoids (*D*) in the presence or absence of pyruvate supplementation or (*E*) upon incubation with MPC inhibitor UK5099. Data were compared by using 2-way ANOVA/Sidak vs paired OCA^{-} controls. $^{*}P \leq .05$, $^{**}P \leq .01$, $^{***}P \leq .001$. OCR, oxygen consumption rate.

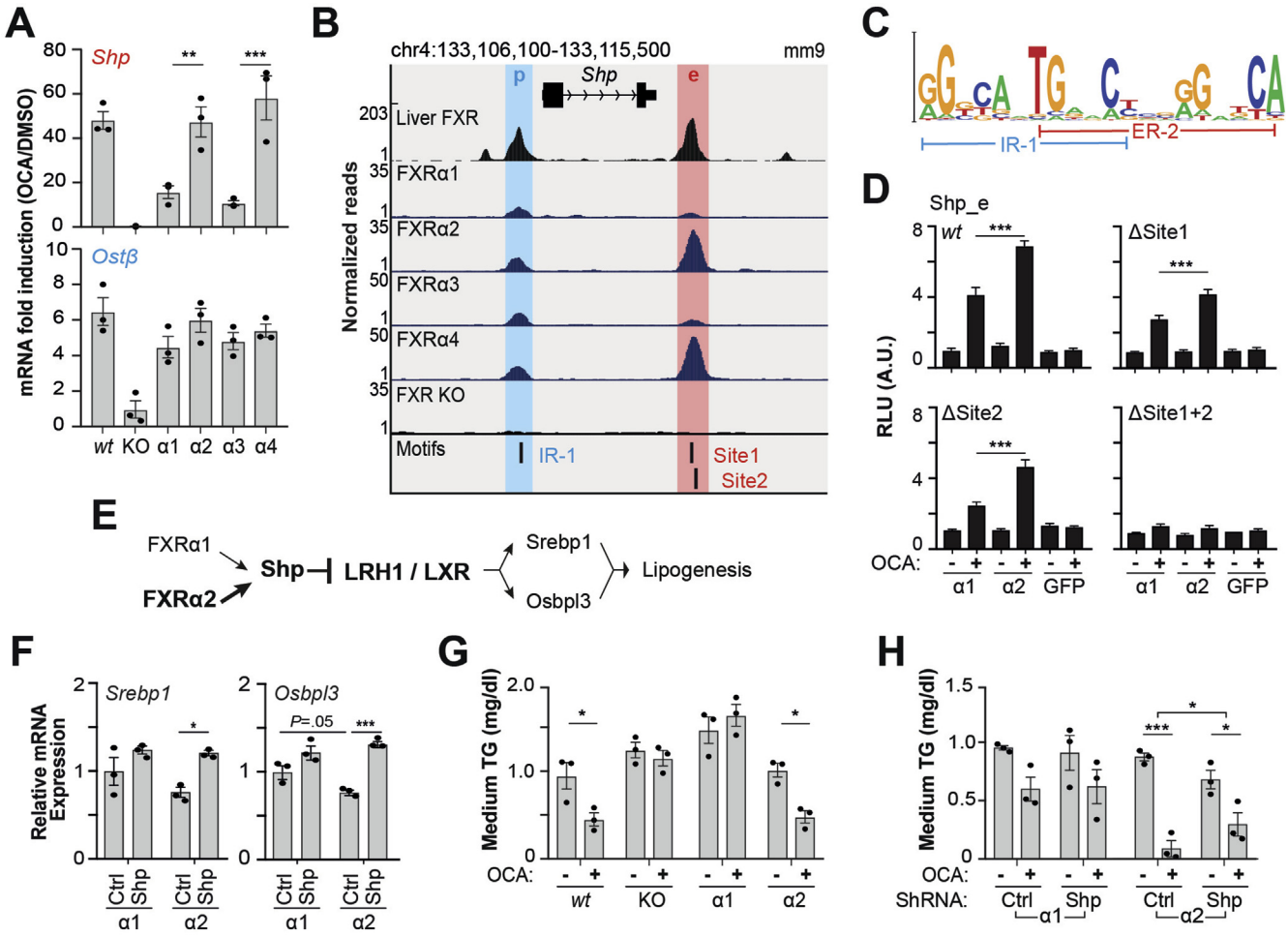

Figure 5. FXRα2-specific up-regulation of *Shp* reduces lipogenesis in liver organoids. (*A*) Induction of FXR target genes upon OCA treatment by RT-qPCR. (*B*) FXR binding in the *Shp* locus in liver and reconstituted *Fxr*$^{-/-}$ (KO) mouse organoids. Promoter (p, containing an IR-1) and enhancer (e, containing IR-1 and ER-2 overlapping sites) regions are highlighted. (*C*) Overlapping motif logo, applicable to sites 1 and 2 in the *Shp* enhancer region. (*D*) Activity of FXRα1 and α2 on luciferase reporters containing the Shp_e region, either wt or upon deletions of the overlapping IR1:ER2 motif sites. (*E*) Proposed mechanism of differential lipid synthesis between FXR isoforms. (*F*) RT-qPCR for regulators of lipogenesis in FXRα1- or FXRα2-expressing organoids upon *Shp* knockdown (n = 3). (*G*) Quantification of TG in medium from wt, *Fxr*$^{-/-}$ (KO), and FXRα1- or FXRα2-expressing organoids. (*H*) Quantification of TG in medium from organoids in which *Shp* was knocked down on FXRα1- or FXRα2-expressing lines. Incubation with OCA is indicated in individual panels. Data were compared using ANOVA/Tukey (*A*, *D*) or 2-way ANOVA/Sidak (*F–H*). *$P \leq .05$, **$P \leq .01$, ***$P \leq .001$. A.U., arbitrary units; Ctrl, control.

Figure 4*C*). The activation pattern from these IR-1:ER-2 motif mutants confirms that the presence of the ER-2 sequence, alone or in overlap with the IR-1 motif, leads to FXRα2-selective transactivation.

Because Shp mediates the FXR-dependent decrease of TG levels through trans-repression of LXR, LRH1, and respective downstream targets[34] (Figure 4*E*), we investigated whether the differential induction of *Shp* expression by FXR isoforms would lead to differences in hepatic lipid metabolism. Of note, FXRα2-transduced organoids express higher levels of Shp compared to FXRα1 in the absence of OCA (Supplementary Figure 5*C*). Expression of the regulators of de novo lipid synthesis *Srebp1* and *Ospbl3*, which are activated by LXR and LRH1,[35,36] was lower in FXRα2-expressing organoids. Moreover, knockdown of *Shp* equalized *Srebp1* and *Ospbl3* expression between FXRα1 and α2 organoids (Figure 5*F* and Supplementary Figure 5*C*). Regarding lipid synthesis and secretion, incubation with OCA promoted a reduction in secreted TG in wt organoids, which was not observed in the absence of FXR (Figure 5*G*). This is analogous to the effect of OCA treatment seen in mice (Supplementary Figure 6*B*). Only FXRα2, but not FXRα1, promoted a similar decrease in TG secretion. Incubation with OCA resulted in a decrease in lipid droplet content in all organoid lines, showing that the reduction observed in secreted TG was not caused by impaired lipid secretion (Supplementary Figure 5*B*). Highlighting the relevance of Shp in FXR isoform–specific response on lipid metabolism, knockdown of *Shp* reduced the effect on TG secretion only in FXRα2-expressing organoids (Figure 5*H*). In conclusion, FXRα2 activates transcription of *Shp* through binding to both IR-1 and ER-2 motifs. This induction mediates, at least

in part, the isoform-specific reduction in hepatic lipogenesis induced by OCA.

FXRα2 Expression Predicts the Regulation From ER-2 Sequences in Human Liver

Given the relevance of FXRα2 expression for ER-2–mediated regulation, we assessed the variation in isoform expression in human liver biopsy samples and commonly used liver cell lines. For this, we analyzed RNA-seq data from histologically normal samples from patients with HCC,[27] PHHs,[28] and HepG2 hepatoma cells. We computed the coverage at the alternative splicing site responsible for the inclusion of the MYTG extension that results in isoforms α1 and α3 and extrapolated this to total FXR expression (Supplementary Table 5). Because FXRα3 and α4 expression levels are low in the liver,[10] we represent the MYTG-containing and -deficient isoforms as FXRα1 and α2, respectively. HepG2 and PHH showed the lowest total FXR expression, with similar expression levels of the FXRα2 and α1 isoforms. In contrast, patients displayed a broad range of both FXR expression and isoform ratios in the liver. In general, those patients with the highest total FXR expression also had the highest FXRα2, but overall FXRα1 was the dominating isoform (Figure 6*A* and Supplementary Figure 6*D*).

With the variability of FXRα2 expression in consideration, we analyzed the expression of candidate IR-1 and ER-2 FXR target genes in the liver biopsy samples in the case of high (quartile [q] 4; q4) or low (q1) *FXR* expression. We found that candidate ER-2–regulated genes, including regulators of carbon and nitrogen metabolism, were higher in q4 compared to q1, whereas IR-1 targets did not share this pattern (Figure 6*B*). With regard to regulators of lipid synthesis, *OSBPL3* expression was lower in q4, consistent with a high expression of *SHP* in this quartile. *SREBP1* showed no significant differences. Interestingly, the livers from $Fxr^{-/-}$ mice also showed increased *Osbpl3*, with no differences in *Srebp1* expression (Supplementary Figure 6*D*). These results indicate that the regulation of *Osbpl3* by Shp, downstream of FXRα2, may contribute to the reduction of hepatic lipogenesis by FXR agonists in vivo.

To determine whether the variations in FXR isoform expression from patients alters binding to IR-1 or ER-2 motifs, we generated HepG2 cell lines overexpressing FXRα1, α2, or GFP. In these cells, we assessed the binding of FXR to regulatory regions within candidate loci (Figure 6*C* and Supplementary Figure 7). The overexpression of FXRα2 resulted in a substantial increase in binding to ER-2 regulatory regions. On the other hand, even at this level of overexpression, FXRα1 did not significantly increase binding to any of the regions tested. We conclude that FXRα2 expression in human liver cells determines the extent of binding to ER-2 regulatory regions and downstream transcriptional activation. Altogether, our results predict that the FXR isoform content in the liver is a primary

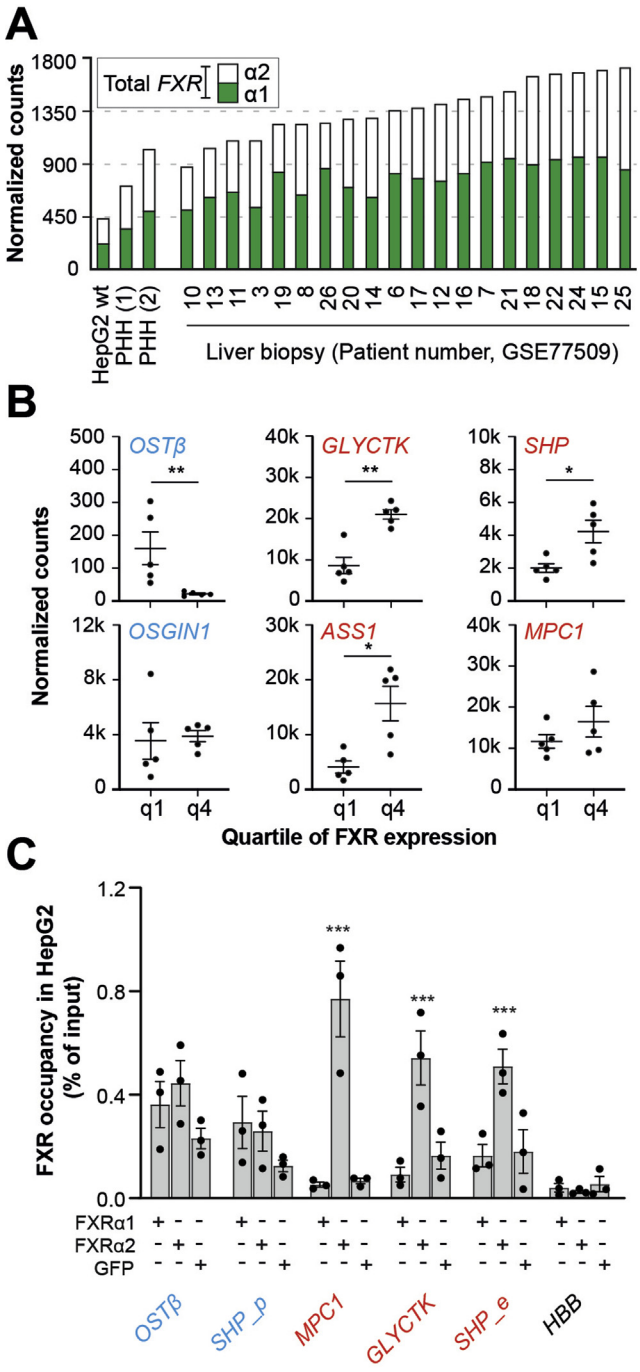

Figure 6. FXRα2 expression predicts the regulation from ER-2 sequences in human liver. (*A*) FXR isoform distribution in HepG2, PHH, and human liver biopsy samples. (*B*) Expression of FXR target genes in human liver biopsy samples in the case of low or high expression of total FXR (n = 5). (*C*) FXR binding to candidate regulatory regions in HepG2 upon overexpression of human FXRα1 or α2. The beta-globin promoter (HBB) was used as negative control. Graphs show (*A*) individual values or (*B*, *C*) average and SEM. ER-2–regulated genes and genomic regions are labeled in red. Data were compared by using (*B*) the Mann-Whitney test or (*C*) 2-way ANOVA/Sidak vs GFP control per locus. $^{*}P \leq .05$, $^{**}P \leq .01$, $^{***}P \leq .001$.

determinant of the extent and characteristics of the response to interventions with FXR ligands.

Discussion

In this study, we have discovered a novel DNA-binding feature of FXR that explains isoform selectivity. FXRα2 and α4 bind genome-wide to a newly identified DNA motif, the ER-2. The ER-2 motif was represented in the majority of sites that were bound by FXR and consequently downgrades binding to the canonical IR-1 motif by all isoforms to a minority of binding events. Even though the IR-1 is the most referenced FXR binding motif,[28] binding to ER-2, or to composite IR-1:ER-2 sites, has been previously reported in mouse and human.[28,37] However, these studies assumed the IR-1 as the central motif, interpreting the extra hexameric repeat in the composite motif as an accessory binding site for additional nuclear receptors. We do not dispute additional binders to these sites, but we conclusively show that FXRα2 and α4 bind to ER-2 sites independently of the presence of an IR-1. FXR isoform specificity has also previously been proposed for variants of the IR-1 motifs, exemplified by the Ibabp promoter.[33] In this report, however, FXRα1 is still shown to bind to the IR-1 and to activate transcription, albeit to a lower extent. We think this difference in transactivation and binding could be the result of a higher permissibility to sequence variations by FXRα2. In our hands, both FXRα1 and α2 activated the IR-1 from the Ibabp promoter at a comparable extent when used in isolation from the rest of the promoter (Supplementary Figure 8). FXRα1 and α2 activated individual IR-1 motifs at varying extents (Supplementary Figure 1*C*), but under no circumstance was FXRα1 bound to or did FXRα1 activate transcription from an ER-2 motif.

Physiologically, the increased relative expression of FXRα2 in the liver after fasting or exercise[12] seems to reflect adaptation of the bile acid response to the existing nutritional status. Here, we show that activation of FXRα2 results in changes in carbon metabolism via newly identified FXR target genes. Through the increase in Mpc1 expression, pyruvate is more efficiently transported into the mitochondria, providing substrates for both anabolic reactions and respiration. Therefore, the activation of FXRα2 in the liver would promote the conversion of pyruvate derived from glycolysis after a meal into energy, lipids, or amino acids.

FXRα2 also selectively enhances the break on de novo lipogenesis. This is of particular importance for nonalcoholic fatty liver disease and NASH treatment, where the estimated contribution of de novo lipid synthesis to hepatic fat content is increased 6-fold in comparison to healthy livers.[38,39] Using the liver organoids as a model, we show that only the activation of FXRα2 led to a reduction in secreted TG. Our data support that a decrease in de novo lipid synthesis is responsible for this effect, at least partially, through enhanced *Shp* activation. This finding is complementary to those presented by Correia et al,[12] further demonstrating the potential of the FXRα2 isoform against liver steatosis: FXRα2 antagonizes the induction of hepatic lipid synthesis by insulin while promoting lipid clearance upon fasting.

Additional identified FXRα2 targets could also contribute to efficient nutrient handling. Glycerate kinase (*Glyctk*) expression promotes the funneling of fructose and glycerates toward glycolysis. In parallel, the induction of *Ass1* expression would allow for the detoxification of ammonia generated from diverse pathways through the urea cycle. In conclusion, the expression and activation of FXRα2 may therefore be crucial in maintaining metabolic health and provide a safeguard against nutrient stress. Interestingly, we noticed that in the livers of mice that were fasted for 4 hours, FXR binding in the *Shp* locus showed high occupancy at the enhancer region and low occupancy at the promoter region. In sharp contrast, occupancy in nonfasted mice was similar in promoter and enhancer regions (Supplementary Figure 5*A*). These observations agree with induced FXRα2 expression upon fasting.[12] Although more experiments are needed to establish causality, this warns for careful documentation of feeding status when assessing the effects of FXR agonism.

Novel FXR target genes *Mpc1* and *Osgin1* promote tumor suppression. Increased Mpc1 is deleterious to tumors where pyruvate metabolism is directed toward lactate production at the expense of mitochondrial respiration.[40] Oxidative stress induced growth inhibitor 1 (Osgin1) is a protein that sensitizes cells to apoptosis upon prolonged oxidative stress.[41] Because MPC1 and OSGIN1 are frequently downregulated in tumor cells and the loss of MPC predicts a poor prognosis in various types of cancer, FXRα2 activation may also have potential in the prevention of HCC.[42,43] The fact that the expression of FXRα2 is highly variable in human livers suggests that the normal physiologic effects of FXR activation, like ammonia detoxification, central carbon metabolism, and the inhibition of de novo lipid synthesis, are also variable. Moreover, liver FXR expression is consistently low in obese patients and those with HCC.[44–47] Although a causal link has not been established, our results show that high liver FXRα2 expression would have a beneficial effect on lipid clearance and cytotoxic and nutrient stresses. A boost in xenobiotic metabolism may undermine drug bioavailability and efficacy; however, the FXRα2 targets annotated in this pathway refer to regular liver functions relevant to energy metabolism (Supplemental Material). The first clinical trials using FXR agonists for the treatment of NASH have shown great potential because hepatic lipid accumulation, fibrosis, and inflammation were shown to be significantly reduced.[48,49] Our data imply that the hepatic FXRα2 expression could be used in the stratification of patients to increase the therapeutic efficacy for NASH. Patients with higher FXRα2 expression in a liver biopsy sample would fully benefit from treatment with FXR ligands, because the subsequent binding to the ER-2 would allow for the regulation of metabolic gene expression. Because the expression of FXR, and FXRα2, in NASH livers and HCC tumors is low overall,[11,44,50] it is expected that ER-2 targets are poorly activated by FXR ligands, missing out on their full therapeutic potential. Prospectively,

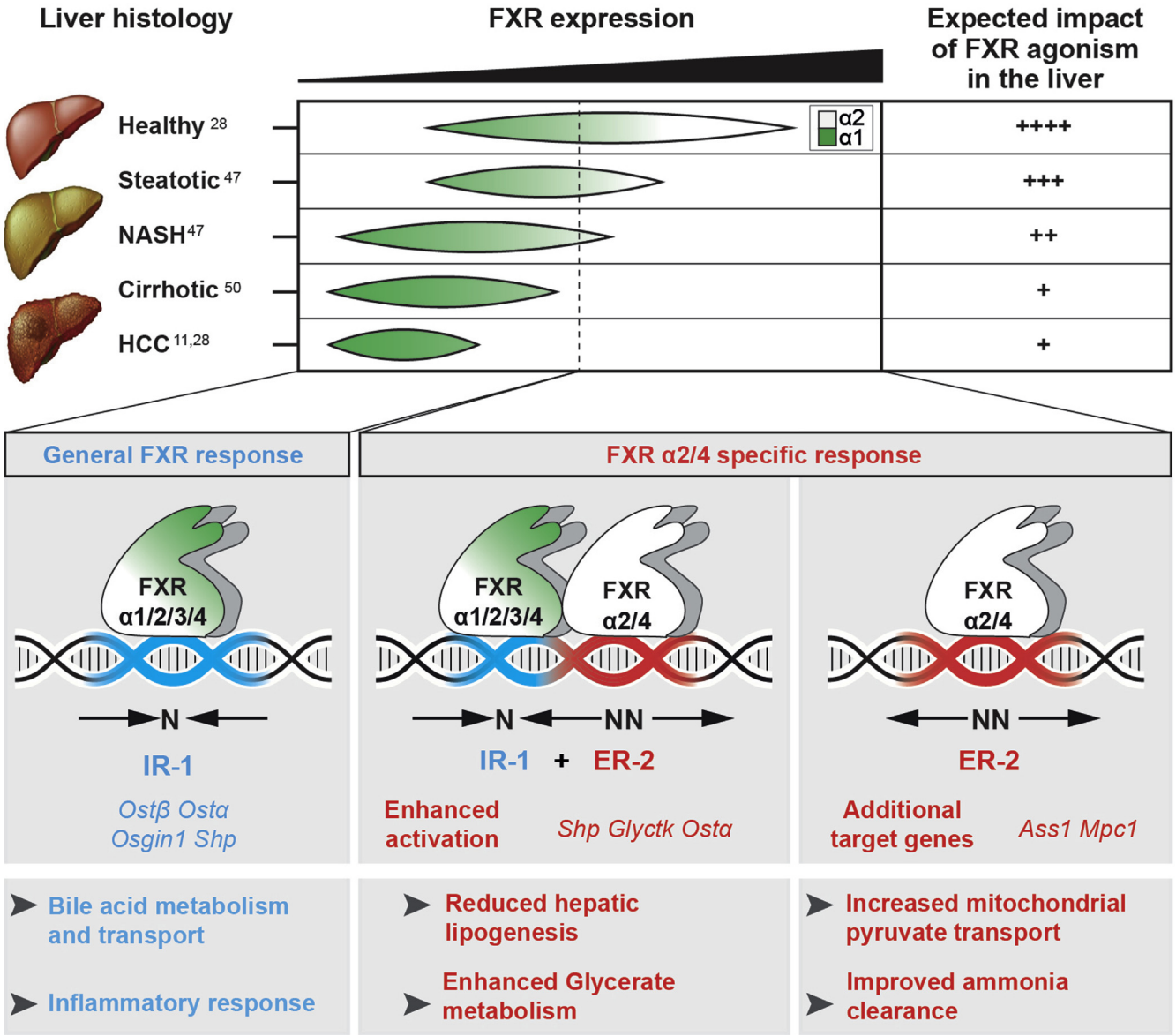

Figure 7. Model for hepatic FXR expression and isoform-specific effects. Schematic representation of the expression of FXR and its isoforms in liver diseases. Patients presenting higher FXRα2 expression in the liver would benefit from FXR agonism through increased transcription of genes regulated through ER-2 motifs.

strategies aimed at increasing FXRα2 expression, and subsequent patient stratification, will increase the therapeutic efficacy of FXR agonists against metabolic diseases (Figure 7).

Supplementary Material

Note: To access the supplementary material accompanying this article, visit the online version of *Gastroenterology* at www.gastrojournal.org, and at https://doi.org/10.1053/j.gastro.2020.07.036.

References

1. Makishima M, Okamoto AY, Repa JJ, et al. Identification of a nuclear receptor for bile acids. Science 1999; 284(5418):1362–1365.
2. Parks DJ, Blanchard SG, Bledsoe RK, et al. Bile acids: natural ligands for an orphan nuclear receptor. Science 1999;284(5418):1365–1368.
3. Wang H, Chen J, Hollister K, et al. Endogenous bile acids are ligands for the nuclear receptor FXR/BAR. Mol Cell 1999;3:543–553.
4. Massafra V, van Mil SWC. Farnesoid X receptor: a "homeostat" for hepatic nutrient metabolism. Biochim Biophys Acta Mol Basis Dis 2018; 1864:45–59.
5. Massafra V, Milona A, Vos HR, et al. Farnesoid X receptor activation promotes hepatic amino acid catabolism and ammonium clearance in mice. Gastroenterology 2017;152:1462–1476.
6. Gadaleta RM, van Erpecum KJ, Oldenburg B, et al. Farnesoid X receptor activation inhibits inflammation and

preserves the intestinal barrier in inflammatory bowel disease. Gut 2011;60:463–472.
7. Bjursell M, Wedin M, Admyre T, et al. Ageing *Fxr* deficient mice develop increased energy expenditure, improved glucose control and liver damage resembling NASH. PLoS One 2013;8(5):e64721.
8. Kim I, Morimura K, Shah Y, et al. Spontaneous hepatocarcinogenesis in farnesoid X receptor-null mice. Carcinogenesis 2007;28:940–946.
9. Zhang S, Wang J, Liu Q, et al. Farnesoid X receptor agonist WAY-362450 attenuates liver inflammation and fibrosis in murine model of non-alcoholic steatohepatitis. J Hepatol 2009;51:380–388.
10. Vaquero J, Monte MJ, Dominguez M, et al. Differential activation of the human farnesoid X receptor depends on the pattern of expressed isoforms and the bile acid pool composition. Biochem Pharmacol 2013;86:926–939.
11. Chen Y, Song X, Valanejad L, et al. Bile salt export pump is dysregulated with altered farnesoid X receptor isoform expression in patients with hepatocellular carcinoma. Hepatology 2013;57:1530–1541.
12. Correia JC, Massart J, de Boer JF, et al. Bioenergetic cues shift FXR splicing towards FXRα2 to modulate hepatic lipolysis and fatty acid metabolism. Mol Metab 2015;4:891–902.
13. Sinal CJ, Tohkin M, Miyata M, et al. Targeted disruption of the nuclear receptor FXR/BAR impairs bile acid and lipid homeostasis. Cell 2000;102:731–744.
14. Huch M, Dorrell C, Boj SF, et al. In vitro expansion of single Lgr5$^+$ liver stem cells induced by Wnt-driven regeneration. Nature 2013;494(7436):247–250.
15. Milona A, Massafra V, Vos H, et al. Steroidogenic control of liver metabolism through a nuclear receptor-network. Mol Metab 2019;30:221–229.
16. Schneider CA, Rasband WS, Eliceiri KW. NIH Image to ImageJ: 25 years of image analysis. Nat Methods 2012; 9:671–675.
17. Ramos Pittol JM, Oruba A, Mittler G, et al. Zbtb7a is a transducer for the control of promoter accessibility by NF-kappa B and multiple other transcription factors. PLoS Biol 2018;16(5):e2004526.
18. Langmead B, Salzberg SL. Fast gapped-read alignment with Bowtie 2. Nat Methods 2012;9:357–359.
19. Zhang Y, Liu T, Meyer CA, et al. Model-based analysis of ChIP-Seq (MACS). Genome Biol 2008;9(9):R137.
20. Ramírez F, Ryan DP, Grüning B, et al. deepTools2: a next generation web server for deep-sequencing data analysis. Nucleic Acids Res 2016;44:W160–W165.
21. Heinz S, Benner C, Spann N, et al. Simple combinations of lineage-determining transcription factors prime cis-regulatory elements required for macrophage and B cell identities. Mol Cell 2010;38:576–589.
22. Zhu LJ, Gazin C, Lawson ND, et al. ChIPpeakAnno: a Bioconductor package to annotate ChIP-seq and ChIP-chip data. BMC Bioinformatics 2010;11:237.
23. Liberzon A, Birger C, Thorvaldsdóttir H, et al. The Molecular Signatures Database (MSigDB) hallmark gene set collection. Cell Syst 2015;1:417–425.
24. Kim D, Pertea G, Trapnell C, et al. TopHat2: accurate alignment of transcriptomes in the presence of insertions, deletions and gene fusions. Genome Biol 2013;14(4):R36.
25. Trapnell C, Hendrickson DG, Sauvageau M, et al. Differential analysis of gene regulation at transcript resolution with RNA-seq. Nat Biotechnol 2013;31:46–53.
26. Ijssennagger N, Janssen AWF, Milona A, et al. Gene expression profiling in human precision cut liver slices in response to the FXR agonist obeticholic acid. J Hepatol 2016;64:1158–1166.
27. Yang Y, Chen L, Gu J, et al. Recurrently deregulated lncRNAs in hepatocellular carcinoma. Nat Commun 2017;8:14421.
28. Zhan L, Liu H-X, Fang Y, et al. Genome-wide binding and transcriptome analysis of human farnesoid X receptor in primary human hepatocytes. PLoS One 2014;9(9): e105930.
29. Edgar R, Domrachev M, Lash AE. Gene Expression Omnibus: NCBI gene expression and hybridization array data repository. Nucleic Acids Res 2002;30:207–210.
30. Anders S, Pyl PT, Huber W. HTSeq—a Python framework to work with high-throughput sequencing data. Bioinformatics 2015;31:166–169.
31. Love MI, Huber W, Anders S. Moderated estimation of fold change and dispersion for RNA-seq data with DESeq2. Genome Biol 2014;15:550.
32. Quinlan AR, Hall IM. BEDTools: a flexible suite of utilities for comparing genomic features. Bioinformatics 2010; 26:841–842.
33. Zhang Y, Kast-Woelbern HR, Edwards PA. Natural structural variants of the nuclear receptor farnesoid X receptor affect transcriptional activation. J Biol Chem 2003;278:104–110.
34. Watanabe M, Houten SM, Wang L, et al. Bile acids lower triglyceride levels via a pathway involving FXR, SHP, and SREBP-1c. J Clin Invest 2004;113:1408–1418.
35. Stein S, Lemos V, Xu P, et al. Impaired SUMOylation of nuclear receptor LRH-1 promotes nonalcoholic fatty liver disease. J Clin Invest 2017;127:583–592.
36. Yan D, Lehto M, Rasilainen L, et al. Oxysterol binding protein induces upregulation of SREBP-1c and enhances hepatic lipogenesis. Arterioscler Thromb Vasc Biol 2007; 27:1108–1114.
37. Thomas AM, Hart SN, Kong B, et al. Genome-wide tissue-specific farnesoid X receptor binding in mouse liver and intestine. Hepatology 2010; 51:1410–1419.
38. Diraison F, Beylot M. Role of human liver lipogenesis and reesterification in triglycerides secretion and in FFA reesterification. Am J Physiol 1998;274(2):E321–E327.
39. Donnelly KL, Smith CI, Schwarzenberg SJ, et al. Sources of fatty acids stored in liver and secreted via lipoproteins in patients with nonalcoholic fatty liver disease. J Clin Invest 2005;115:1343–1351.
40. Schell JC, Olson KA, Jiang L, et al. A role for the mitochondrial pyruvate carrier as a repressor of the Warburg effect and colon cancer cell growth. Mol Cell 2014; 56:400–413.
41. Hu J, Yao H, Gan F, et al. Interaction of OKL38 and p53 in regulating mitochondrial structure and function. PLoS One 2012;7(8):e43362.

42. Liu M, Li Y, Chen L, et al. Allele-specific imbalance of oxidative stress-induced growth inhibitor 1 associates with progression of hepatocellular carcinoma. Gastroenterology 2014;146:1084–1096.
43. Ma X, Cui Y, Zhou H, et al. Function of mitochondrial pyruvate carriers in hepatocellular carcinoma patients. Oncol Lett 2018;15:9110–9116.
44. Nobili V, Alisi A, Mosca A, et al. Hepatic farnesoid X receptor protein level and circulating fibroblast growth factor 19 concentration in children with NAFLD. Liver Int 2018;38:342–349.
45. Su H, Ma C, Liu J, et al. Downregulation of nuclear receptor FXR is associated with multiple malignant clinicopathological characteristics in human hepatocellular carcinoma. Am J Physiol Gastrointest Liver Physiol 2012; 303:G1245–G1253.
46. Liu N, Meng Z, Lou G, et al. Hepatocarcinogenesis in $FXR^{-/-}$ mice mimics human HCC progression that operates through HNF1α regulation of FXR expression. Mol Endocrinol 2012;26:775–785.
47. Nie H, Song C, Wang D, et al. MicroRNA-194 inhibition improves dietary-induced non-alcoholic fatty liver disease in mice through targeting on FXR. Biochim Biophys Acta 2017;1863:3087–3094.
48. Neuschwander-Tetri BA, Loomba R, Sanyal AJ, et al. Farnesoid X nuclear receptor ligand obeticholic acid for non-cirrhotic, non-alcoholic steatohepatitis (FLINT): a multicentre, randomised, placebo-controlled trial. Lancet 2015;385(9972):956–965.
49. Loomba R, Sanyal AJ, Kowdley KV, et al. Factors associated with histologic response in adult patients with nonalcoholic steatohepatitis. Gastroenterology 2019; 156:88–95.
50. More VR, Cheng Q, Donepudi AC, et al. Alcohol cirrhosis alters nuclear receptor and drug transporter expression in human liver. Drug Metab Dispos 2013;41:1148–1155.

Received October 7, 2019. Accepted July 21, 2020.

Correspondence
Address correspondence to: Prof. Saskia W.C. van Mil. Center for Molecular Medicine UMC Utrecht, Stratenum building, HP 3.217. PO box 85060, 3508AB Utrecht, The Netherlands. e-mail: S.W.C.vanMil@umcutrecht.nl.

Acknowledgments
The authors thank Nico Lansu and Noortje van den Dungen (Epigenomics Facility) and the Utrecht Sequencing Facility for the preparation of sequencing libraries and Illumina sequencing, Ingrid Bijsmans for the extraction of liver organoids, and Maaike Meerlo (Metabolomics Expertise Center, University Medical Center Utrecht) for technical assistance with bioenergetic measurements. Intercept Pharmaceuticals is acknowledged for the gift of obeticholic acid. The authors thank Boudewijn Burgering, Alexander Heberle, and Stefanía Magnúsdóttir for critically reviewing the manuscript.

CRediT Authorship Contributions
Jose Miguel Ramos Pittol, PhD (Conceptualization: Equal; Formal analysis: Lead; Investigation: Lead; Methodology: Lead; Project administration: Equal; Supervision: Supporting; Writing – original draft: Equal); Alexandra Milona, PhD (Investigation: Supporting; Methodology: Supporting); Imogen Morris, MSc (Investigation: Supporting; Methodology: Supporting); Ellen C.L. Willemsen, BSc (Investigation: Supporting; Methodology: Supporting); Suzanne W. van der Veen, BSc (Investigation: Supporting; Methodology: Supporting); Eric Kalkhoven, PhD (Methodology: Supporting; Project administration: Supporting); Saskia W.C. van Mil, PhD (Conceptualization: Equal; Funding acquisition: Lead; Project administration: Equal; Supervision: Lead; Writing – original draft: Equal).

Conflicts of interest
The authors disclose no conflicts.

Funding
This work was financially supported by Marie Skłodowska-Curie Actions of the European Commission (PIAPP-GA-2013-611979) and the European Union's Horizon 2020 Marie Skłodowska-Curie Innovative Training Network, Tribbles Research and Innovation Network (TRAIN) (project no. 721532).

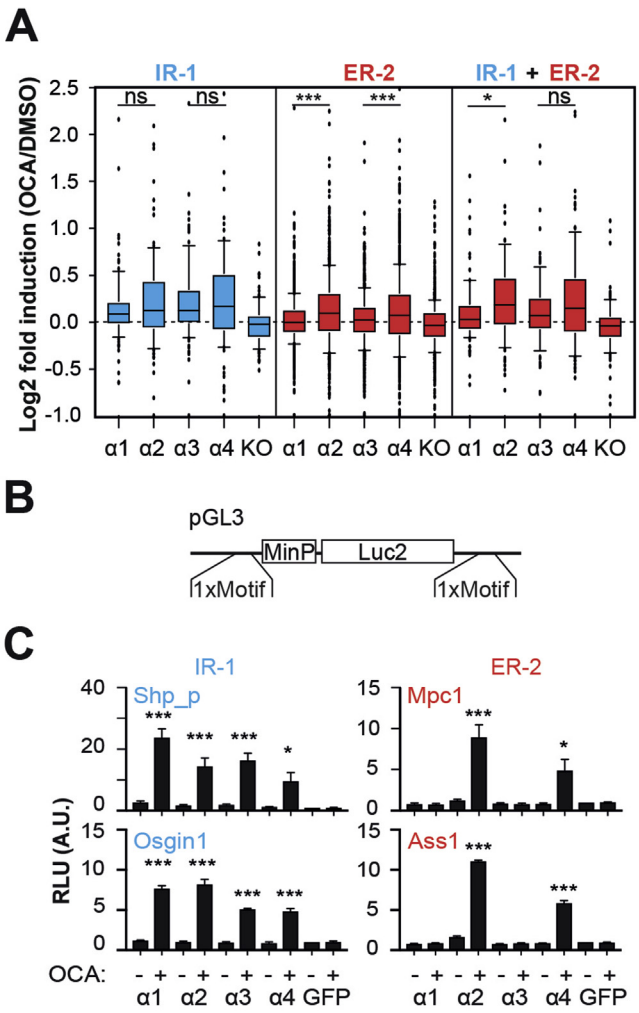

Supplementary Figure 1. (*A*) RNA fold induction of genes with neighboring FXR bound regions containing an IR-1, ER-2, or both motifs after treatment with OCA. n = 105 (IR-1), n = 734 (ER-2), and n = 104 (both). Bars represent the 10th–90th percentiles. (*B*) Schematic representation of motif insertion in luciferase reporter constructs. (*C*) Luciferase reporter assays using human FXR isoforms in the indicated native motif reporter constructs. Graphs show group average and standard error of the mean, n = 3. Data were compared using (*A*) Kruskal-Wallis *H* test or (*C*) ANOVA/Sidak vs paired OCA^{-}. $^{*}P \leq 0.05$, $^{***}P \leq .001$. A.U., arbitrary units; ns, not significant.

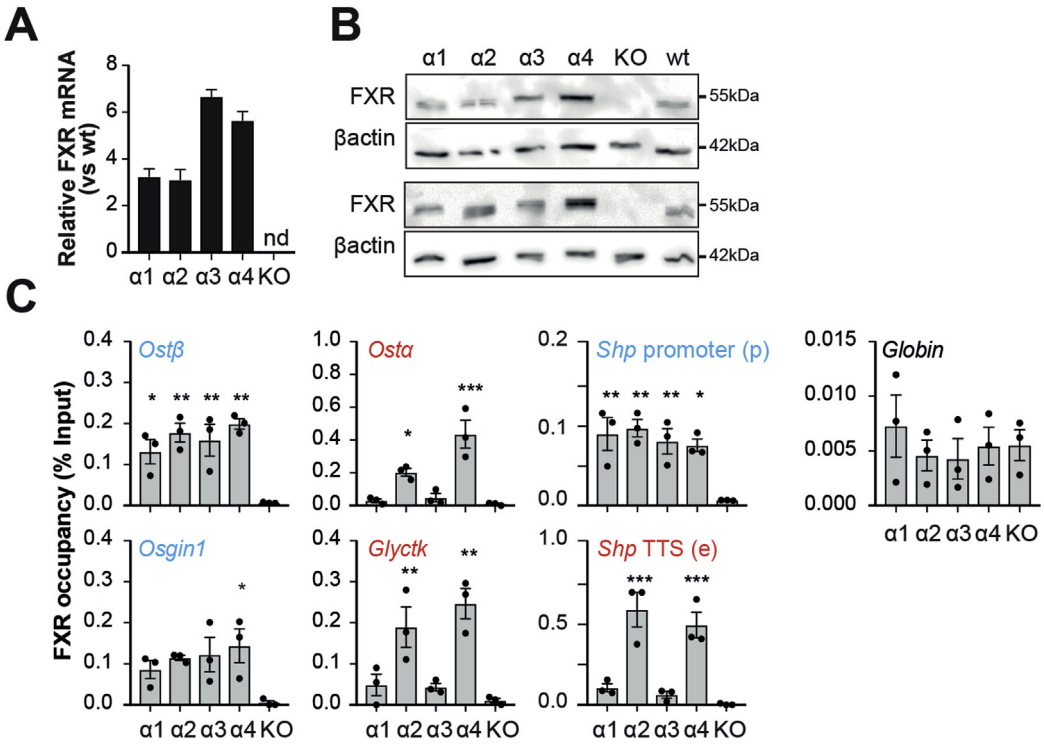

Supplementary Figure 2. (*A*) *Fxr* expression by qPCR on reconstituted organoids. (*B*) Western blot for FXR and β-actin on liver organoid lines from 2 independent transduction rounds. (*C*) FXR occupancy at selected genomic loci by ChIP-qPCR. Graphs show (*A*) group averages and standard deviation or (*C*) individual data points, average, and standard error of the mean, n = 3. Data were compared using ANOVA/Sidak vs KO (*C*). $^{*}P \leq .05$, $^{**}P \leq .01$, $^{***}P \leq .001$.

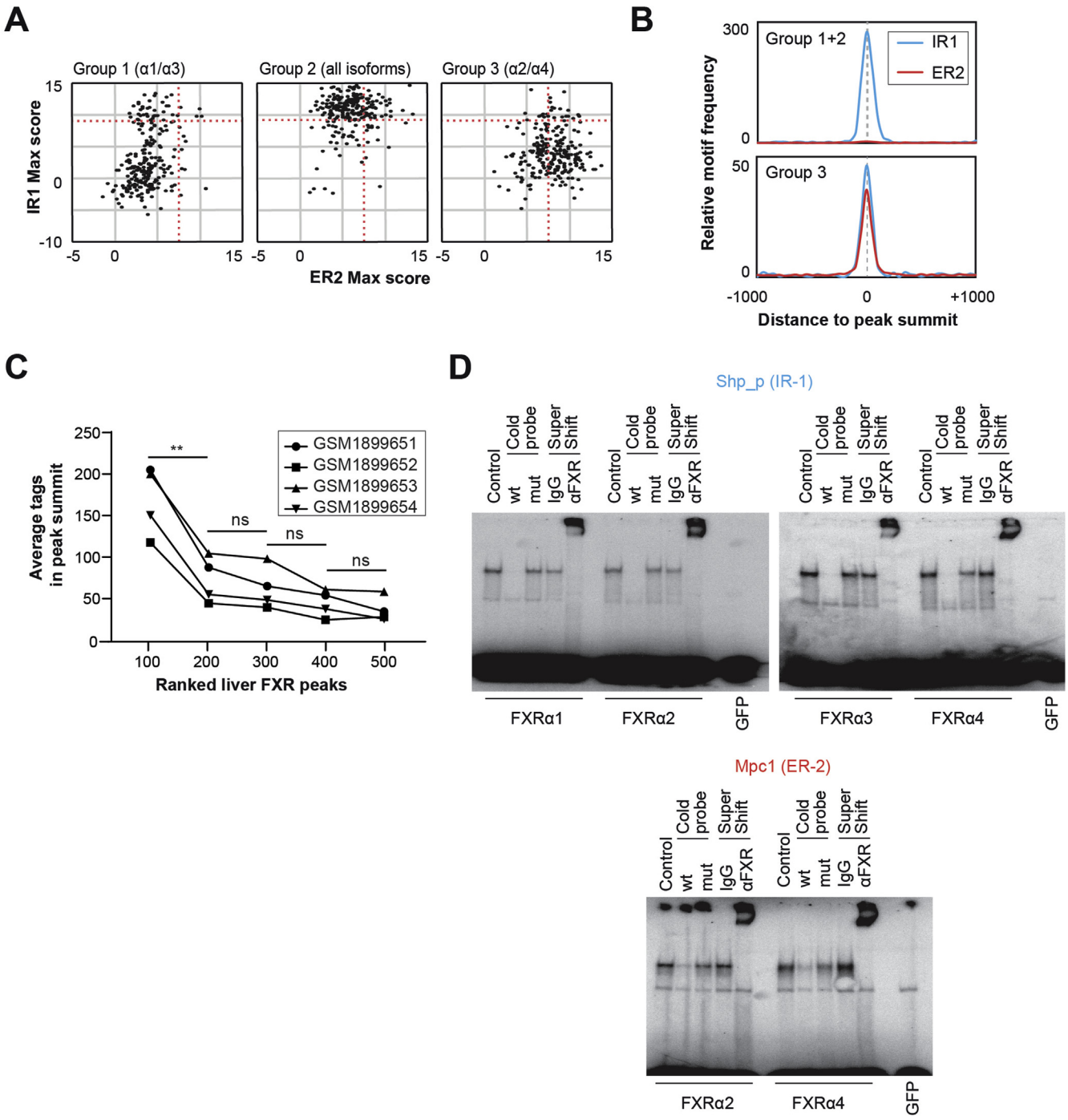

Supplementary Figure 3. (*A*) Max IR-1 vs ER-2 motif score on 150 random FXR peaks per group assigned by overlap in binding among the FXR isoforms. HOMER threshold scores are marked in red (IR-1 = 9.45, ER-2 = 7.99). (*B*) Localization of IR-1 and ER-2 motifs within FXR peaks, divided by group. Frequency was normalized to the values calculated for the surrounding 500 base pairs up- and downstream from the FXR peak. (*C*) Average number of tags at the summit in FXR ChIP-seq data sets from mouse liver (GSE73624), sorted by statistical ranking. Data were compared by using ANOVA/Sidak vs the following peak rank. (*D*) Electromobility shift assay specificity and binding controls. $^{**}P \leq .01$. Max, maximum; ns, not significant.

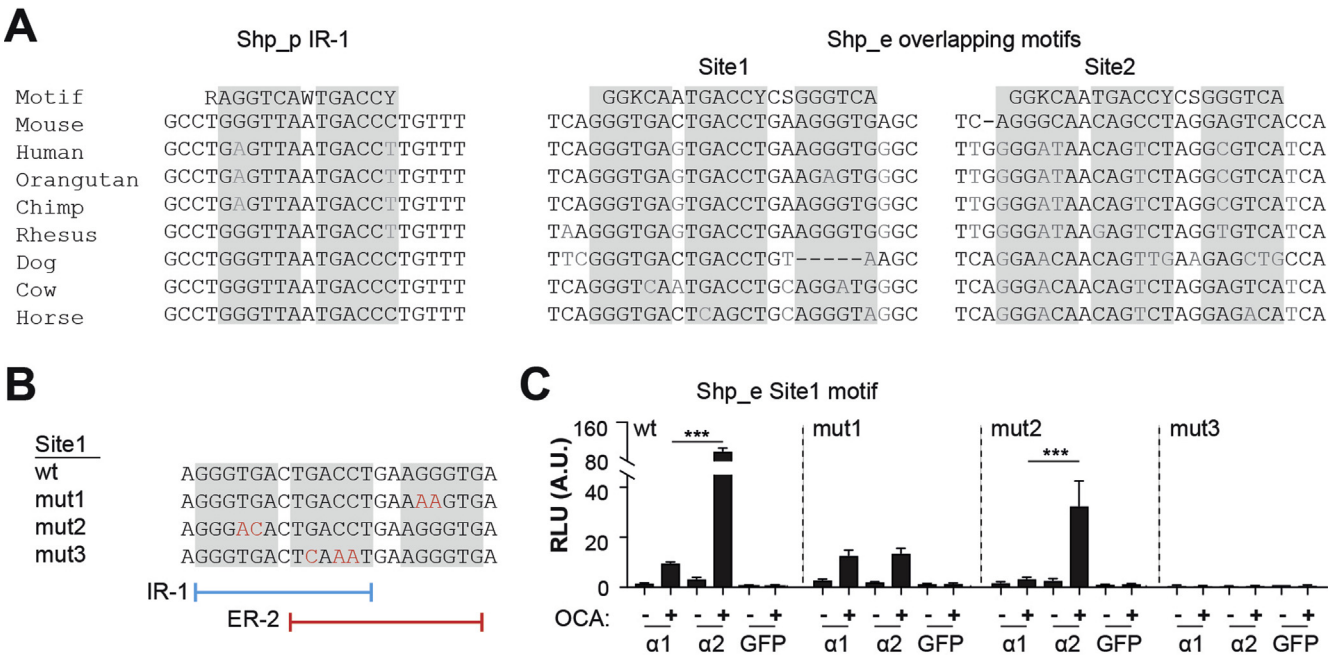

Supplementary Figure 4. (*A*) Species comparison of FXR binding motifs in the Shp_p and Shp_e regions. Hexameric repeats are highlighted in gray. Mouse motif was used as reference. (*B*) Shp_e site 1 sequence and inactivating mutations tested (*marked in red*) in the 3 hexameric repeats (*highlighted in gray*). (*C*) Luciferase assay on Shp_e site1 wt and mutant motifs. Graphs show group average and standard error of the mean, n = 3. Data were compared by using 2-way ANOVA/Sidak α1 vs α2. ***$P \leq .001$.

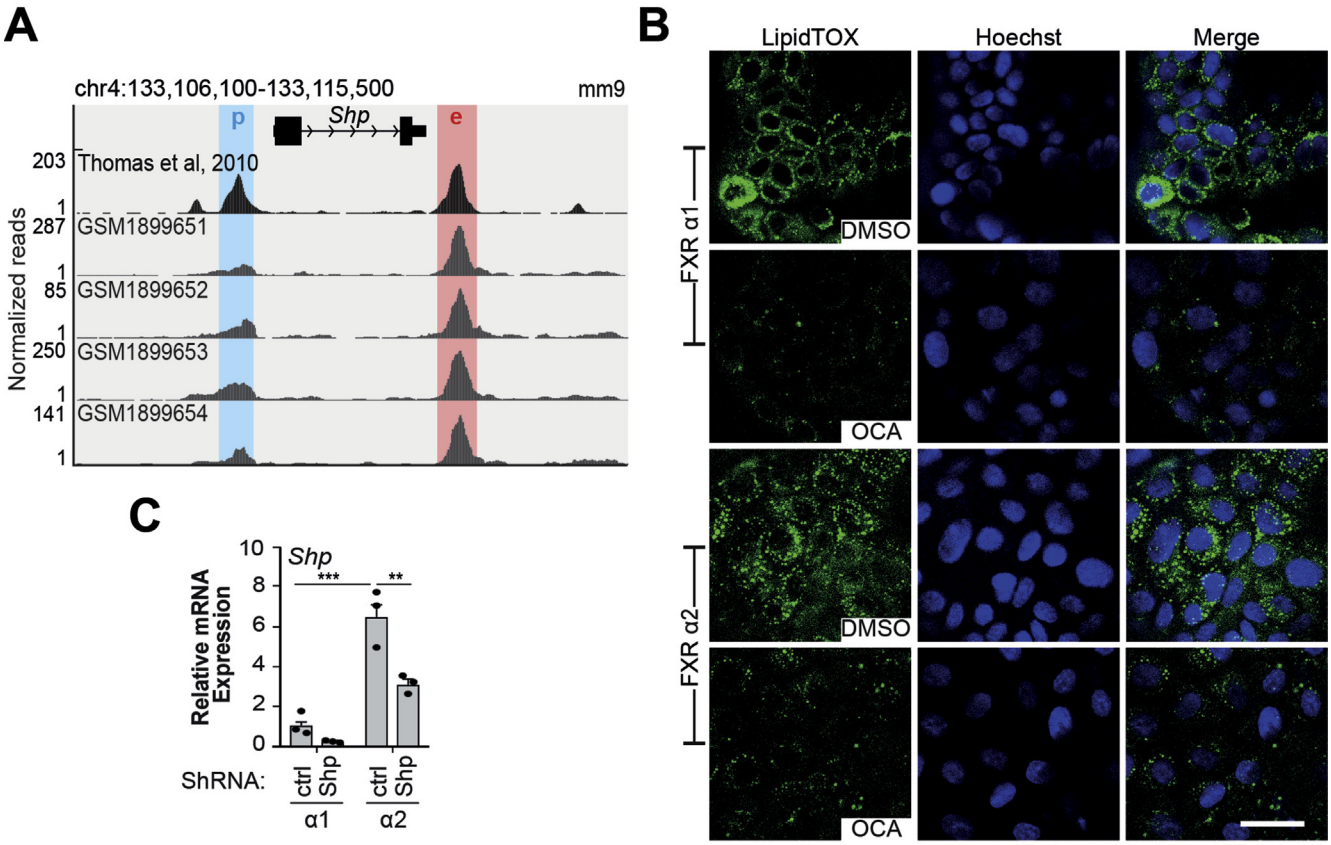

Supplementary Figure 5. (*A*) FXR binding in the *Shp* locus in the liver from fasted vs nonfasted mice (GSE73624 vs Thomas et al,[37] respectively). (*B*) LipidTOX staining of lipid droplets in DMSO- or OCA-treated liver organoids expressing FXRα1 or α2. Scale bar = 25 μm. (*C*) *Shp* expression by reverse-transcription qPCR in FXRα1- or FXRα2-expressing organoids upon *Shp* knockdown (n = 3). Data were compared by using 2-way ANOVA/Sidak (*C*). $^{**}P \leq .01$, $^{***}P \leq .001$. ctrl, control.

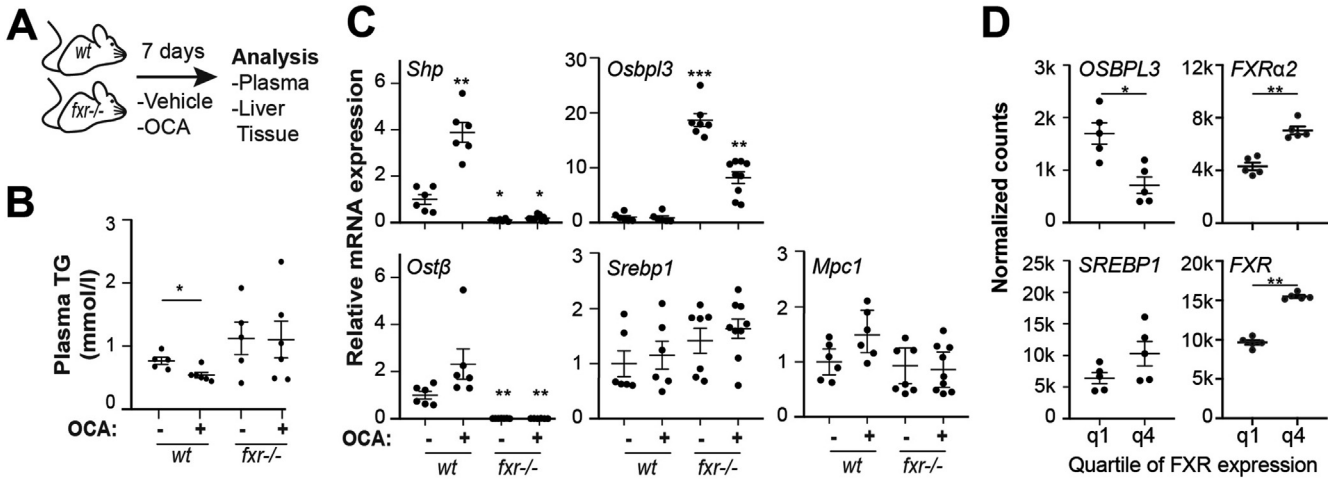

Supplementary Figure 6. (*A*) Schematic representation of mouse experiment. (*B*) Quantification of plasma TG in OCA- or vehicle-treated mice. n = 5 (vehicle), n = 6 (OCA). (*C*) RT-qPCR on FXR targets and lipid synthesis regulators and *Mpc1* in mouse liver tissue, n = 6 (wt vehicle and OCA), n = 7 ($Fxr^{-/-}$ vehicle), n = 9 ($Fxr^{-/-}$ OCA). (*E*) Expression of lipid synthesis regulators and *FXR* in human liver biopsy samples in case of low (q1) or high (q4) expression of FXR (n = 5). Data were compared using (*B*, *C*) Brown-Forsythe and Welch ANOVA/Dunnett T3 vs wt vehicle or (*D*) Mann-Whitney test. $^{*}P \leq 0.05$, $^{**}P \leq 0.01$, $^{***}P \leq 0.001$. q, quartile.

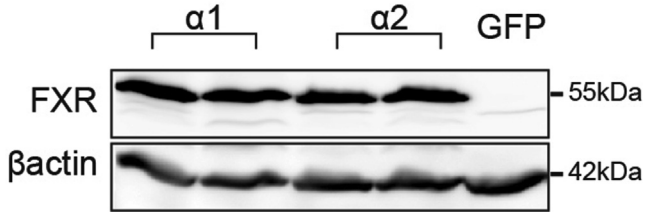

Supplementary Figure 7. Western blot for FXR and βactin on HepG2 overexpressing human FXRα1, FXRα2, or GFP.

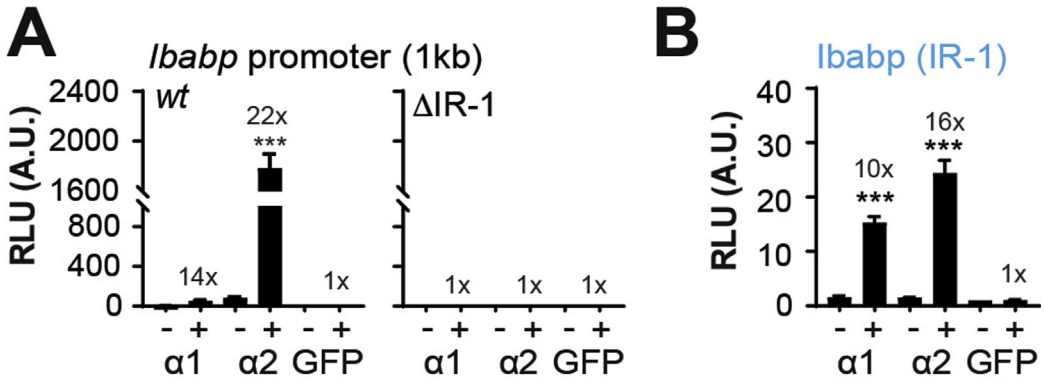

Supplementary Figure 8. (*A*) Luciferase reporter assays using the mouse Ibabp promoter, either wt or upon deletion of the IR-1. (*B*) Luciferase reporter assays using exclusively the IR-1 from the Ibabp promoter as described in Supplementary Figure 1*B*. Data were compared using ANOVA/Sidak vs paired OCA^{-}. ***$P \leq .001$. ns, not significant.

Supplementary Table 1. Regions and Motifs Used for Luciferase Reporter Constructs[a]

Genomic regions					
Identifier	Motif	Chromosome number	Start	End	
Shp_e	Site1 + site 2	4	133113322	133113688	
Ibabp_pro	IR-1	11	43415063	43416093	
Individual motifs					
ID	Motif	Chromosome number	Start	End	Sequence
Ass1	ER-2	2	31320333	31320356	GGTC***TGGCCT***GG***AGGTCA***TTCT
Mpc1	ER-2	17	8477278	8477301	CAAG***TGACCG***AG***CGGACA***GCGC
Osgin1	IR-1	8	121960922	121960942	ACA***AGTTCA***T***TCACCC***AGGG
Fasn	IR-1	11	120686032	120686053	GCG***CGGTCG***T***TGACCC***TGGC
Ibabp	IR-1	11	43415191	43415208	TA***AGGTGA***A***TAACCT***TG
Shp_p	IR-1	4	133108979	133109000	ACT***GGGTTA***A***TGACCC***TGTT
Shp_e Site1	ER-2 + IR-1	4	133113420	133113444	CA***GGGTGA***C***TGACCT***GA***AGGGTG***AG
Shp_e Site2	ER-2 + IR-1	4	133113584	133113608	TC***AGGGCA***A***CAGCCT***AG***GAGTCA***CC

[a]Hexameric elements are highlighted in bold italic font. Coordinates correspond to the mm9 genomic assembly.

Supplementary Table 2. Statistical Significance of Overlaps in DNA Binding Among FXR Isoforms

Rank	α1	α2	α3	α4	*P* value
1	+	−	+	−	5.61×10^{-57}
2	−	+	−	+	1.54×10^{-40}
3	−	+	+	−	1.70×10^{-16}
4	+	+	−	−	1.50×10^{-11}
5	−	−	+	+	>.99
6	+	−	−	+	>.99

Supplementary Table 3. Primer Probes Used for Electrophoretic Mobility Shift Assay Experiments[a]

Identifier	Forward	Reverse
Fasn	GCG***CGGTCG***T***TGACCC***TGGC	GCCA***GGGTCA***A***CGACCG***CGC
Shp_p	CCT***GGGTTA***A***TGACCC***TGTT	AACA***GGGTCA***T***TAACCC***AGG
Shp_p mutant	CCT***GGGTTA***ATGAaaCTGTT	AACAGttTCAT***TAACCC***AGG
Ass1	GTC***TGGCCT***GG***AGGTCA***TTC	GAA***TGACCT***CC***AGGCCA***GAC
Mpc1	AAG***TGACCG***AG***CGGACA***GCG	CGC***TGTCCG***CT***CGGTCA***CTT
Mpc1 mutant	AAGTGAaaGAG***CGGACA***GCG	CGC***TGTCCG***CTCttTCACTT

[a]Hexameric elements are highlighted in bold italic font. Inactivating mutations are noted in lowercase.

Supplementary Table 4. Primers Used for qPCR for the Quantification of Transcript Abundance or the Binding of FXR to Regulatory Regions

Identifier	Forward	Reverse
Reverse-transcription qPCR primers for mouse transcripts		
Srebp1	GAACAGACACTGGCCGAGAT	GAGGCCAGAGAAGCAGAAGAG
Shp	CGATCCTCTTCAACCCAGATG	AGGGCTCCAAGACTTCACACA
Ostβ	AGATGCGGCTCCTTGGAATTA	TGGCTGCTTCTTTCGATTTCTG
Osbpl3	ATTACCACCCACCGACACTC	CTCGATCCTCTGCTTCTGAAC
Mpc1	TGAATAGCCGAGAGTCCCTAAA	TGATGAAGACAAATAAGGTTTAGCA
Ppia	GGAGATGGCACAGGAGGAA	GCCCGTAGTGCTTCAGCTT
ChIP-qPCR primers for mouse genomic DNA		
Ostβ_promoter	TGGGCTCCTGGCACTTTCGG	TGGGACTTCAGGCTGGGTGG
Osta_promoter	CAGCTCCCTCTTGCCCTCC	TAGACAGTTCACCATGTCTCTTGAGTCC
Osgin1_promoter	CCTGCTGACTCACGCTTATG	AAGGCTAGCAGGGGTATTTCA
Glyctk_promoter	CCTCCTAGGTCACCTCCTTTG	CAGGATGTGGAAGAAGAATGG
Shp_promoter	CATGGAAATGGGCATCAATA	CGTGGCCTTGCTATCACTTT
Shp_enhancer	AGCAGTTGTCTACAGGGCTTTC	CGGTGAGAAGGATCCAAACT
βGlobin_promoter	CCTGCCCTCTCTATCCTGTG	GCAAATGTGTTGCCAAAAAG
ChIP-qPCR primers for human genomic DNA		
OSTβ_promoter	GGTGCTTTCGGATTGTGAA	CAGGGTGACTGACCTCTTGAA
MPC1_promoter	GACACCAGACCCCGAGTG	GGGGTGTCATTGGCTCTG
GLYCTK_promoter	GGCTATGGGCTCAGTTATGG	ACCACCCACAGTGGTGAGA
SHP_promoter	GGTCATTAACTCAGGCTGTACCA	GGACACCTGCTGATTGTGC
SHP_enhancer	GGAGGCCGGAAAATCCTAT	GTCAGGGTGAGTGACCTGAAG
HBB_promoter	TGGCTCTGCCCTGACTTTTA	AGGGTTGGCCAATCTACTCC

Supplementary Table 5. Coverage at the Alternative Splicing Donor Boundary (±MYTG) at the FXR Locus From RNA-Seq in Human Cell Lines and Liver Biopsy Samples[a]

ID	Accession	$\alpha1 + \alpha2$ counts chromosome 12 position 100926376	$\alpha1$ counts chromosome 12 position 100926377	$\alpha2$ fraction	Total FXR normalized counts
HepG2 samples (GSE133659)					
Wt	SRX6387618	13	7	0.46	433.42
*FXRα1	SRX6387624	137	133	0.03	8218.88
*FXRα2	SRX6387630	63	0	1.00	4767.67
PHH samples (GSE57227)					
1	SRX530187	172	83	0.52	1242.30
2	SRX530188	107	53	0.50	1016.39
Patient samples (GSE77509)					
3	SRR3140234	66	32	0.52	1096.04
6	SRR3140239	88	53	0.40	1354.18
7	SRR3140244	89	55	0.38	1472.13
8	SRR3140249	68	35	0.49	1237.43
10	SRR3140254	48	28	0.42	869.71
11	SRR3140259	203	121	0.40	1092.16
12	SRR3140264	97	52	0.46	1400.20
13	SRR3140269	111	66	0.41	1034.11
14	SRR3140274	103	49	0.52	1284.97
15	SRR3140279	135	76	0.44	1697.65
16	SRR3140284	323	182	0.44	1448.86
17	SRR3140289	218	123	0.44	1376.29
18	SRR3140295	151	82	0.46	1645.96
19	SRR3140299	109	73	0.33	1234.99
20	SRR3140303	125	68	0.46	1278.97
21	SRR3140307	135	84	0.38	1517.45
22	SRR3140311	141	79	0.44	1663.92
24	SRR3140315	147	84	0.43	1672.47
25	SRR3140320	85	42	0.51	1711.66
26	SRR3140326	121	84	0.31	1242.30

[a]Reads were assigned to FXRα1 and α2 because human liver predominantly expresses these isoforms. HepG2 overexpressing FXRα1 or α2 were used as validation for the quantification method. Coordinates correspond to the hg19 genomic assembly.

Supplementary Table 6. Motif Abundance (Percentage of Peaks) in FXR Peaks From Mouse Liver, Sorted by Statistical Significance of FXR Enrichment Over Input Material

			Ranked liver FXR peaks, %				
GEO accession number	Treatment	Motif	1–100	101–200	201–300	301–400	401–500
GSM1899651	OCA	IR-1	76	52	39	51	49
GSM1899652	OCA	IR-1	52	65	56	55	53
GSM1899653	Vehicle	IR-1	65	52	58	53	54
GSM1899654	Vehicle	IR-1	57	49	44	44	38
GSM1899651	OCA	ER-2	65	50	60	46	36
GSM1899652	OCA	ER-2	69	47	45	46	38
GSM1899653	Vehicle	ER-2	68	60	51	47	51
GSM1899654	Vehicle	ER-2	66	46	49	43	41